RESEARCH ARTICLE

WILEY | PRIMATOLOGY

Loss of ferritin-positive microglia relates to increased iron, RNA oxidation, and dystrophic microglia in the brains of aged male marmosets

Juan de Dios Rodríguez-Callejas[1] | Daniel Cuervo-Zanatta[1] |
Abraham Rosas-Arellano[1] | Caroline Fonta[2] | Eberhard Fuchs[3] |
Claudia Perez-Cruz[1] (ID)

[1] Department of Pharmacology, Center of
Research in Advance Studies, Mexico City,
Mexico

[2] Brain and Cognition Research Centre
(CERCO), CNRS/University of Toulouse,
Toulouse, France

[3] German Primate Center, Leibniz Institute for
Primate Research, Göttingen, Germany

Correspondence
Claudia Perez-Cruz, Laboratory of
Neuroplasticity and Neurodegeneration,
Department of Pharmacology, Center of
Research in Advance Studies, Av. Politécnico
Nacional 2508, Col. San Pedro Zacatenco,
07360 Mexico City, Mexico.
Email: cperezc@cinvestav.mx

Funding information
Consejo Nacional de Ciencia y Tecnología,
Grant number: 308515

Microglia are cells that protect brain tissue from invading agents and toxic substances, first by releasing pro-inflammatory cytokines, and thereafter by clearing tissue by phagocytosis. Microglia express ferritin, a protein with ferroxidase activity capable of storing iron, a metal that accumulates in brain during aging. Increasing evidence suggests that ferritin plays an important role in inflammation. However, it is not known if ferritin/iron content can be related to the activation state of microglia. To this end, we aimed to delineate the role of ferritin in microglia activation in a non-human primate model. We analyzed brains of male marmosets and observed an increased density of ferritin+ microglia with an activated phenotype in hippocampus and cortex of old marmosets (mean age 11.25 ± 0.70 years) compared to younger subjects. This was accompanied by an increased number of dystrophic microglia in old marmosets. However, in aged subjects (mean age 16.83 ± 2.59 years) the number of ferritin+ microglia was decreased compared to old ones. Meanwhile, the content of iron in brain tissue and cells with oxidized RNA increased during aging in all hippocampal and cortical regions analyzed. Abundant amoeboid microglia were commonly observed surrounding neurons with oxidized RNA. Notably, amoeboid microglia were arginase1+ and IL-10+, indicative of a M2 phenotype. Some of those M2 cells also presented RNA oxidation and a dystrophic phenotype. Therefore, our data suggest that ferritin confers protection to microglia in adult and old marmosets, while in aged subjects the decline in ferritin and the increased amount of iron in brain tissue may be related to the increased number of cells with oxidized RNA, perhaps precluding the onset of neurodegeneration.

KEYWORDS
aging, Callithrix jacchus, cortex, hippocampus, non-human primate

1 | INTRODUCTION

Common marmosets have gained popularity as a biomedical model due to their ability to provide a good anatomical and pathophysiological representation of the human central nervous system (Tardif, Mansfield, Ratnam, Ross, & Ziegler, 2011; T'Hart, Abbott, Nakamura, & Fuchs, 2012). For aging studies, they are attractive candidates because of a shorter life span than other non-human primates, as marmoset onset of aging starts around 8 years of age (Abbott & Barnett, 2003; Ross & Salmon, 2018; Tardif et al., 2011). One key

phenotype as the brain ages is an aberrant innate immune response characterized by neuroinflammation. Microglia are the key mediators of innate immunity in brain (Ransohoff & Perry, 2009) and can be in a resting or in an activated state (Kettenmann, Hanisch, Noda, & Verkhratsky, 2011). Resting microglia constantly survey their environment, ready to support endangered neurons or interfere with a potential threat to the tissue integrity (Nimmerjahn, Kirchhoff, & Helmchen, 2005). Danger signals may cause transformation of microglia into an activated state, referred to as M1 and M2 subtypes (Tang & Le, 2016). M1 activation is associated with inflammatory response (Moehle & West, 2015), while M2 phagocytic/neuro-protective state is induced by signals from apoptotic cells and plays a role in remodeling and repair (Hanisch & Kettenmann, 2007). M2 microglia is characterized by an upregulation of arginase-1 (Arg1) and the release of neurotrophic factors (Cherry, Olschowka, & O'Banion, 2015). In aged brains, microglia is rather dystrophic, senescent, and associated with decreased ability to reach a normal response to injury (von Bernhardi, Eugenín-von Bernhardi, & Eugenín, 2015). Dystrophic microglia display morphological changes, such as an amoeboid shape, fewer and shorter processes, cytoplasm fragmentation or cytorrhexis, and formation of spheroid swellings (Streit, Braak, Xue, & Bechmann, 2009; Streit, Sammons, Kuhns, & Sparks, 2004). These senescent microglia co-localize with degenerating neurons, losing their homogeneous tissue distribution, and accumulating phagocytic inclusions (Hart, Wyttenbach, Hugh Perry, & Teeling, 2012; Hefendehl et al., 2014; Tremblay, Zettel, Ison, Allen, & Majewska, 2012). Dystrophic microglia are described in old humans (Streit et al., 2004), aged marmoset (Rodriguez-Callejas, Fuchs, & Perez-Cruz, 2016), and neurodegenerative conditions such as Alzheimer's Disease (AD) (Lopes, Sparks, & Streit, 2008; Streit et al., 2009). Aged rodents (28 months of age) do not exhibit dystrophy of microglia as observed in AD brains, a condition related to their shorter life-span compared to humans (Streit, Xue, Tischer, & Bechmann, 2014). Moreover, transgenic mice models of AD, which accumulates amyloid beta peptides, do develop a robust activation state of microglia around amyloid plaques but not dystrophy (Jimenez et al., 2008; Moreno-Gonzalez et al., 2009; Navarro et al., 2018). On the contrary, hyperphosphorylated tau protein, a hallmark of AD, can be detected in adolescent and aged marmosets in dystrophic microglia (Rodriguez-Callejas et al., 2016). However, the cause of microglia dystrophy remains unclear.

In old humans and AD patients, ferritin has been proposed to be a marker of dystrophic microglia (Lopes et al., 2008). Ferritin plays an essential role in iron homeostasis as it can uptake/reuse iron and store it for a long term. Iron deficiency or excess is harmful for the brain (Arosio, Ingrassia, & Cavadini, 2009; Chasteen & Harrison, 1999) and iron accumulation seems to be present in several neurodegenerative conditions (Ramos et al., 2014; Smith, Harris, Sayre, & Perry, 1997; Ward, Zucca, Duyn, Crichton, & Zecca, 2014; Zecca, Youdim, Riederer, Connor, & Crichton, 2004). Thus, if iron storage in ferritin complex prevents iron-induced increase in oxidative stress (Balla et al., 1992; Cermak et al., 1993; Guan et al., 2017; Lin & Girotti, 1998; Orino et al., 2001; Wang et al., 2011) then, it may confer a neuroprotective effect

to cells. Moreover, oxidative stress leads to RNA oxidation, a condition associated with age-related brain pathologies (Kong & Lin, 2010), such as AD (Nunomura et al., 1999, 2001; Nunomura, Moreira et al., 2012; Shan & Lin, 2006; Smith, Rottkamp, Nunomura, Raina, & Perry, 2000), amyotrophic lateral sclerosis (Chang et al., 2008), dementia with Lewy bodies (Nunomura et al., 2001), psychiatric disorders (Che, Wang, Shao, & Young, 2010), Parkinson's disease (Zhang et al., 1999), among others. Therefore, we hypothesized that ferritin will confer protection to activated microglia against increased oxidative stress during aging. We evaluated ferritin, oxidative stress, iron content, and microglia phenotype in brain of male marmosets during aging. Based on previous descriptions of the brain areas affected in neurodegenerative diseases associated with aging (Braak, Alafuzoff, Arzberger, Kretzschmar, & Tredici, 2006; Braak & Braak, 1991, 1995) we analyzed hippocampal (CA1-CA3 and dentate gyrus) and cortical areas (temporal, parietal, and entorhinal cortex). Our results showed that while iron tissue content increased through adult life, the number of microglia labeled with iron decreased in aged (mean age 16.83 ± 2.59 years) marmosets. RNA oxidation also increased in all the brain regions analyzed along aging. Most microglia did not show RNA oxidation, but in old aged marmosets few microglia had damaged RNA. In hippocampus of old and aged marmoset (mean age 11.25 ± 0.7 years) we observed amoeboid shaped microglia expressing Arg1 and Interleukin-10 (IL-10), indicative of activated M2 type. Nonetheless, some M2 microglia presented RNA oxidation and a dystrophic phenotype. Given this, we propose that ferritin confers protection to activated microglia, whereas decreased ferritin and increased iron tissue content in brain of aged marmoset can be associated with enhanced RNA oxidation and dystrophy of microglia.

2 | METHODS

2.1 | Subjects

Laboratory-bred common marmosets (*Callithrix jacchus*) were housed at the German Primate Center, Göttingen, Germany, under standard conditions complying with the European Union guidelines for the accommodation and care of animals used for experimental and other scientific purposes (2007/526/EC). All animal experiments were performed in accordance with the German Animal Welfare Act, which strictly adheres to the European Union guidelines (EU directive 2010/63/EU) on the use of non-human primates for biomedical research. Experienced veterinarians and caretakers constantly monitored the animals. Animals did not present neurological disorders or other injuries that can cause trauma to the central nervous system.

2.2 | Tissue preparation

Brains of male marmosets of different ages were used in the current study: Four adolescent (A: mean age 1.75 ± 0.18 years), three adults (Ad: mean age 5.33 ± 0.88 years), six old (O: mean age 11.25 ± 0.70 years), and three aged (Ag: mean age 16.83 ± 2.59 years) individuals based on previous age classification (Abbott and Barnett, 2003) were investigated. Animals were anesthetized with an i.p. injection (0.1 ml/100 g

body weight) of GM II (ketamine, 50 mg/ml; xylazine 10 mg/ml; atropin 0.1 mg/ml) and after loss of consciousness they received an i.p. injection of ketamine (400 mg/kg body weight). Bodies were transcardially perfused with cold (4 °C) saline (0.9 % NaCl) for 5 min. Subsequently, for fixation of the brains, cold (4 °C) 4 % paraformaldehyde (PFA) in 0.1 M phosphate buffer, pH 7.2, was infused for 15 min. The brains were removed and post fixed in fresh 4 % PFA at 4 °C, where brains were stored until sectioning. Before sectioning, tissue was washed thoroughly with 0.1 M phosphate buffered saline (PBS: 0.15 M NaCl, 2.97 mM Na_2HPO_4-$7H_2O$, 1.06 mM KH_2PO_4; pH 7.4), and immersed in 30 % sucrose in PBS at 4 °C four days before sectioning. Coronal sections (40 μm thick) were obtained using a sliding microtome (Leica RM2235) and we prepared series every 6th section (at interval of 240 μm) from the medial temporal area (TEM), inferior and superior parietal lobe (PAR), entorhinal cortex (ENT), and hippocampal formation (Bregma 8.00 mm to 0.80 mm) according to Paxinos et al. (2012) (Figure 1). Sections were

immediately immersed in cryoprotectant solutions, one for light microscopy [300 g sucrose; 400 ml 0.1M PBS, and 300 ml ethylene glycol, for 1 L] and other for immunofluorescence [300 g sucrose; 10 g polyvinyl-pyrrolidone (PVP-40); 500 ml of 0.1M PBS and 300 ml ethylene glycol, for 1 L] and stored at −20 °C until use.

2.3 | Immunoperoxydase staining

Brain slices were permeabilized with 0.2 % Triton X100 in PBS (0.2 % PBS-triton) for 20 min. Sections were then rinsed in PBS and incubated in 0.3 % hydrogen peroxide (H_2O_2) in PBS for 10 min to inactivate endogenous peroxidase activity. The following washing steps were performed 3 times, 10 min each, in 0.2 % PBS-triton. To block potential nonspecific antibody binding, sections were incubated in 5 % bovine serum albumin (BSA, Sigma) in PBS for 15 min (for 8-hydroxyguano-sine, 8OHG), or 0.1 % BSA by 30 min (for ferritin). Subsequently, sections were incubated overnight at 4 °C with the primary antibodies: anti-8OHG or anti-ferritin (all primary and secondary antibodies used in this study are summarized in Supplementary Table S1) diluted in 0.2 % PBS-triton. Brain slices were thoroughly washed in 0.2 % PBS-triton and incubated for 2 hr at room temperature (RT) with secondary horseradish peroxidase-conjugated antibodies (see Supplementary Table S1) in 0.2 % PBS-triton. Hydrogen peroxide (0.01 %) and the chromogen 3,3′-diaminobenzidine (DAB, 0.06 %) in 0.2 % PBS-triton were used to develop the horseradish peroxidase enzymatic reaction. The enzymatic reaction was stopped with 0.2 % PBS-triton and then sections were mounted on glass slides and left to dry overnight. Dry sections were cover slipped with mounting medium Entellan (Merck).

2.4 | Immunofluorescence

Brain slices were permeabilized with 0.2 % Triton X100 in PBS (0.2 % PBS-triton) by 20 min. For epitope reactivation, the tissue was exposed to concentrated formic acid (89.8 %) for 15 min and then to boiling citrate buffer (SSC Buffer, 20× Concentrate Sigma-Aldrich, 95 °C) for 10 min. For blocking antigenic sites, the tissue was exposed to 2 % BSA. Thereafter, sections were incubated with glial-fibrillary acidic protein antibody (anti-GFAP, Supplementary Table S1) overnight in 0.05 % PBS-triton. Immunoreactivity was evidenced by use of secondary antibody diluted in 2 % BSA for 4 hr at RT. Finally, all slices were exposed to 4,6-diamidine-2-phenylindole (DAPI, 1:500) in tris-buffered saline (TBS) for 45 min and then mounted with Vectashield (Vector Laboratories).

2.5 | Double labeling immunofluorescence

Brain slices were permeabilized with 0.2 % PBS-triton by 20 min. Thereafter, sections were treated with 0.1 % BSA in PBS by 30 min and incubated overnight at 4 °C with the first primary antibody. Then, sections were rinsed with 0.2 % PBS-triton, and incubated 2 hr at RT with the corresponding secondary antibody (see Supplementary Table S1) diluted in 0.2 % PBS-triton. In a next step, brain slices were washed with 0.2 % PBS-triton and the process was repeated for the second primary antibody (see Supplementary Table S1). All sections were co-incubated with DAPI (1:1000, Invitrogen) in 0.2 %
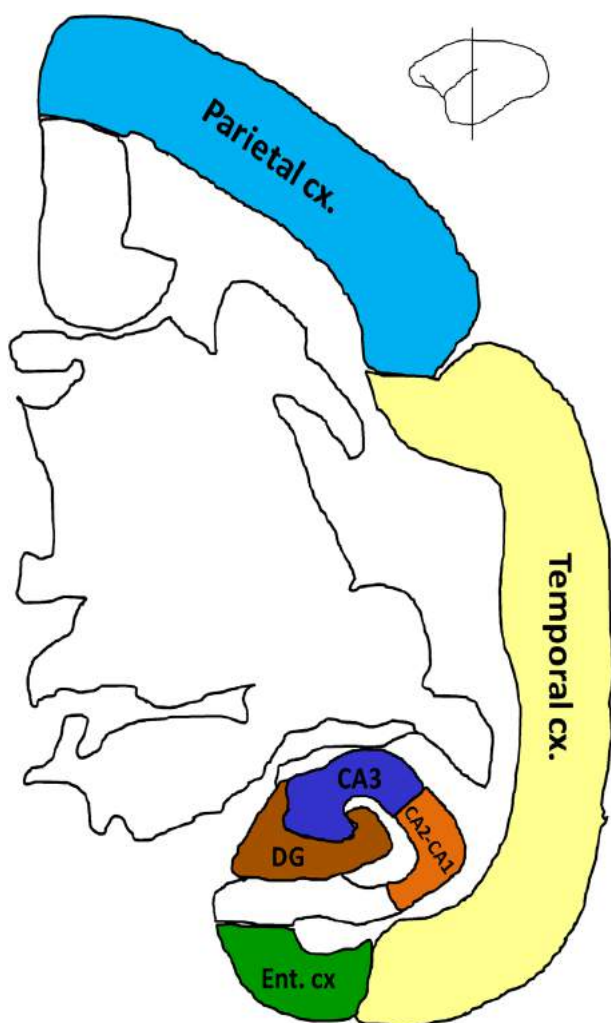

FIGURE 1 Hippocampal and cortical regions of marmoset brain analyzed in the current study. Hippocampal regions: CA3, CA2-CA1, and Dentate Gyrus (DG). Cortical regions: Parietal (PAR), Temporal (TEM), and Entorhinal (ENT) cortices. Adapted from Paxinos et al. (2012)

PBS-triton during 30 min. The sections were then washed and mounted on glass slides. Dry sections were cover slipped with mounting medium VectaShield (Vector Laboratories).

2.6 | Multiple labeling immunofluorescence using antibody signal enhancer (ASE)

Signal amplification was obtained by use of antibody signal enhancer (ASE) method as previously described (Rosas-Arellano et al., 2016), for Arg1 and IL-10 antibodies. Briefly, sections were rinsed with 0.5 % PBS-Tween20 twice for 3 min. To block potential nonspecific antibody binding, sections were incubated for 30 min using a solution containing 2 % donkey serum, 50 mM glycine, 0.05 % Tween20, 0.1 % TritonX-100 and 0.1 % BSA diluted in PBS. Primary antibodies were incubated in ASE solution, consisting 10 mM glycine, 0.05 % Tween20, 0.1 % TritonX-100, and 0.1 % hydrogen peroxide in PBS, and left overnight at 4 °C (see antibodies specifications in Supplementary Table S1). On the next day, sections were washed with 0.5 % PBS-Tween20, and thereafter, incubated with secondary antibody (see Supplementary Table S1) diluted in 0.1 % PBS-Tween20 for 2 hr at RT. Sections were then rinsed before the standard double labeling immunofluorescence (see Section 2.7) begin, with a second primary antibody (anti-8OHG, anti-Iba1, or anti-ferritin) as described above.

2.7 | Histochemical detection of iron

Iron histochemical detection was performed according to Sands et al. (2016). First, slices were incubated in a solution of 1 % potassium ferrocyanide trihydrate (Sigma-Aldrich)/5 % PVP (Sigma-Aldrich)/0.05N HCl for 60 min. Sections were washed with ultrapure water and incubated in methanol containing 0.01M sodium azide (Sigma-Aldrich) and 0.3 % H_2O_2 for 75 min. In a next step, sections were washed with PBS and incubated in a solution of 10 mg DAB/160 ml 30 % H_2O_2/40 ml 0.01M Tris HCl (pH 7.4) for 2 min and sections were thoroughly rinsed with PBS. For double staining with ferritin antibody, slices were permeabilized with 0.2 % PBS-triton during 20 min and incubated in 0.1 % BSA for 30 min. Sections were rinsed 3 times with 0.2 % PBS-triton (10 min each) and incubated overnight at 4 °C with anti-ferritin antibody (see Supplementary Table S1). After washing, sections were incubated 2 hr at RT with biotilynated secondary antibody (see Supplementary Table S1). Subsequently, sections were incubated with the avidin-biotin complex (ABC Kit; Vector Laboratories) in 0.2 % PBS-triton for 2 hr at RT, according to the producer's instructions. Finally, antibody binding was visualized with DAB (Peroxidase Substrate Kit; Vector Laboratories) 0.025 %, with 0.01 % H_2O_2 as a catalytic agent. Control sections were processed without the primary antibody. The sections were then washed, mounted on glass slides and left to dry overnight. Dry sections were cover slipped with mounting medium Entellan (Merck).

2.8 | Image acquisition

Nikon Eclipse 80i light microscope equipped with a Nikon DS-Ri1 camera was used to acquire bright-field images under 10× (for 8OHG),

20×, and 100× (for ferritin and iron) objectives. For fluorescent labeling, images were obtained by a confocal microscope (Leica TCS-SP8) with argon (488 nm), and helium/neon (543 nm) lasers. Both lasers were always used with optimized pinhole diameter. For GFAP quantifications, a 20× objective was used performing optical scanning each 2.07 μm in Z axis, projected and analyzed in a two-dimensional plane. For double labeling image acquisition, 20× and 100× objectives were used. All confocal images were obtained as z-stacks of single optical sections. Stacks of optical sections were superimposed as a single image by using the Leica LAS X software. Depending on the staining, 2 or 3 slices were used for each subject (see Section 2.9). Those slices were used to obtain images from different regions of the hippocampus (dentate gyrus [DG], cornu ammonis 3 [CA3], and CA2-CA1) and cortical regions (entorhinal, ENT, temporal, TEM, and parietal, PAR) according to the marmoset brain atlas (Paxinos et al., 2012) (Figure 1).

2.9 | Morphometry

Labeling with anti-ferritin antibody was used to assess microglial phenotypes. Ferritin labels microglia and oligodendrocytes, but neurons are not labeled. Oligodendrocytes immunoreactive to ferritin present a specific morphology readily differentiated from microglia, as they showed small and round soma, with only one or two processes (Lopes et al., 2008) (Figure 2B). Microglia quantification and classification was assessed in ferritin+ microglia, readily identified according to their morphology (Lopes et al., 2008). Based on previous descriptions, cellular and morphological characteristics were classified as: resting (displaying a slight ramified morphology and small rounded soma), activated (hypertrophic soma and ramified cells with extensively thick and branched processes), and dystrophic cells (loss of fine branches, presence of shortened tortuous processes and/or cytoplasmic fragmentation) (Rodriguez-Callejas et al., 2016; Streit et al., 2009, 2004). We used three slices per subject to obtain 3 images from DG, 5 images from CA3, 4 images from CA2-CA1 hippocampal areas, and 4 images from ENT cortex, 6 images from TEMP and 6 images from PAR from each slice. The number of microglia with different morphological features per area (number of cells/number of images × single image area 0.276 mm^2) was scored in each brain region. Furthermore, in CA2-CA1 region of old marmoset, activated microglia were classified in two types: Highly ramified (with hypertrophied cytoplasm and highly ramified long processes) and ameboid (with hypertrophied cytoplasm and short ramified processes). ImageJ software (NIH, Bethesda, Maryland) was used to classify activated microglia. Functions "plugins"— "analyze"—"cell counter" were used. The number of highly ramified and amoeboid activated microglia was scored, and their densities calculated (number of cells/number of images × single image area).

Number of astrocytes (GFAP+) was quantified in at least three slices per subject. From each slice we obtained three images from the each region of interest (DG, CA3, CA2-CA1, and ENT C×). GFAP+ cells were quantified by use of ImageJ software plugins ITCN: Imaging-based tool for counting nuclei (ITCN) which makes use of average cell
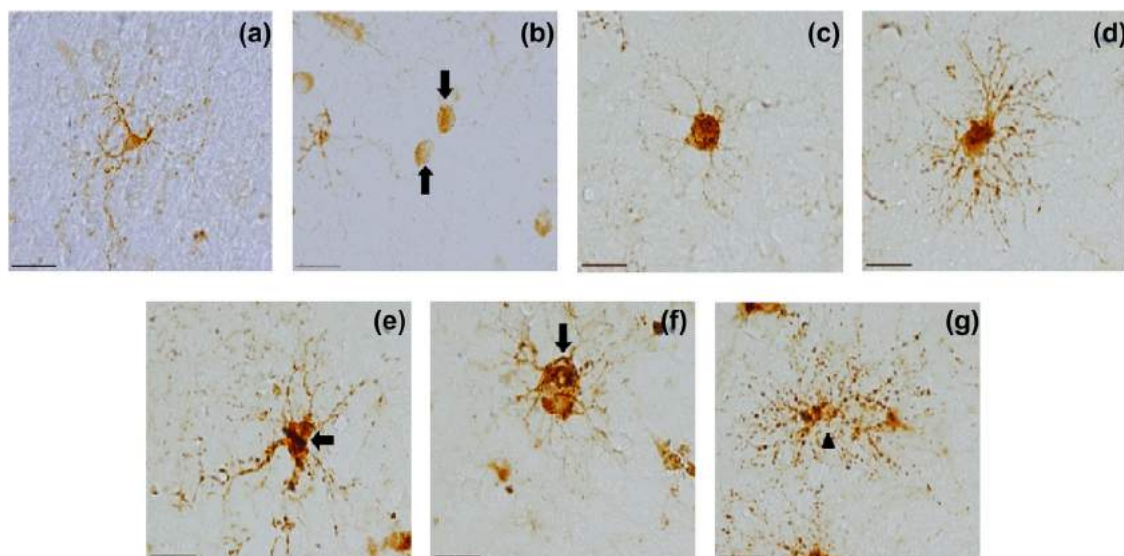
FIGURE 2 Representative photomicrographs of oligodendrocyte and microglia phenotypes using anti-ferritin antibody. (a) Resting microglia with small cytoplasm and thin ramified processes. (b) Oligodendrocytes (arrows) show a round cytoplasm without processes. (c) Ameboid activated microglia characterized by hypertrophied cytoplasm and short ramified processes. (d) Highly ramified activated microglia characterized by hypertrophied cytoplasm and long ramified processes. (e-g) Dystrophic microglia with de-ramified tortuous processes (arrows) and cytoplasm fragmentation (cythorrexis, arrowhead). Note the hypertrophic soma in active microglia (c and d) compared to resting microglia (a). Scale bar 20 μm

diameter, inter-cell minimum distance and detection threshold; whereas GFAP body size was assessed by ImageJ software plugin Wand: Screening tool for detecting cell body maximum threshold and isolating it from background and non-specific staining.

To quantify the percentage of area covered with specific staining (i.e., number of 8OHG+ cells, the percentage of area stained with iron; and microglia positive to iron [microglia + iron]) two brain slices per subject were used. The following images were obtained from each slice: 3 images from DG, 3 images from CA3, 3 images from CA2-CA1, 3 images from ENT, 10 images from TEM, and PAR cortices. The total stained area covered from each region was calculated as the total number of images multiplied by the area of a single image (1105440 μm² for 8OHG-ir and 276360 μm² for microglia+ iron). ImageJ software was used to determine the area covered by 8OHG-ir and iron-positive cells. To determine the percentage of staining in a determined region, the sum of the areas covered by 8OHG+ or iron were divided by the total area, and then, multiplied by 100. To quantify number of microglia+ iron per area, ImageJ cell counter function was used. Cells were selected if they showed microglial morphology and colocalization with iron and ferritin labeling (Figure 4, dark blue stained cells). Iron content in tissue, and the number of microglia+ iron was calculated in each region as follows: iron content or total number of microglia + iron per region/number of images × single image area 0.276 mm².

2.10 | Statistical analysis

Using GraphPad Prism 6.0 software, statistical analysis was performed by one-way ANOVA, followed by a Tukeýs as posthoc test, except the comparison of activated microglia subtype when an unpaired-T test was used. Differences were considered statistically significant when $p ≤ 0.05$. Data are presented as means ± S.E.M.

3 | RESULTS

3.1 | Ferritin positive microglia increased in adult and old marmoset but decreased in aged subjects

Representative images of ferritin+ cells in hippocampus (DG, CA3, and CA2-CA1 regions) and ENT cortex are shown in Figure 2. We observed that ferritin+ microglia was present at all ages, being more abundant in adult and old marmosets, compared to young and aged animals, especially in *stratum oriens* of CA3 and CA2-CA1 (Figure 3a). In addition, in adult and old marmosets, ferritin+ microglia appear larger (hypertrophic) and more ramified, both characteristics of an activated microglia (Ransohoff & Perry, 2009; Streit et al., 2004) (Figure 3a).

The quantification of ferritin+ microglia indicates that the density of resting and activated microglia decreased in hippocampus and cortex of aged marmoset compared to old ones. Dystrophic microglia increased in old marmoset compared to adolescent animals in all regions analyzed, but it is slightly reduced in aged subjects (Figuress 3b and 7, Table 1). Therefore, microglia labeled with ferritin showed that the activation state peaks in adult and old individuals, but it is diminished in aged marmoset. A similar trend was observed for resting and dystrophic microglia in aged marmoset (Table 1).

Iba-1 antibody has been widely used to labeled microglia (Imai, Ibata, Ito, Ohsawa, & Kohsaka, 1996; Ito et al., 1998). In a previous
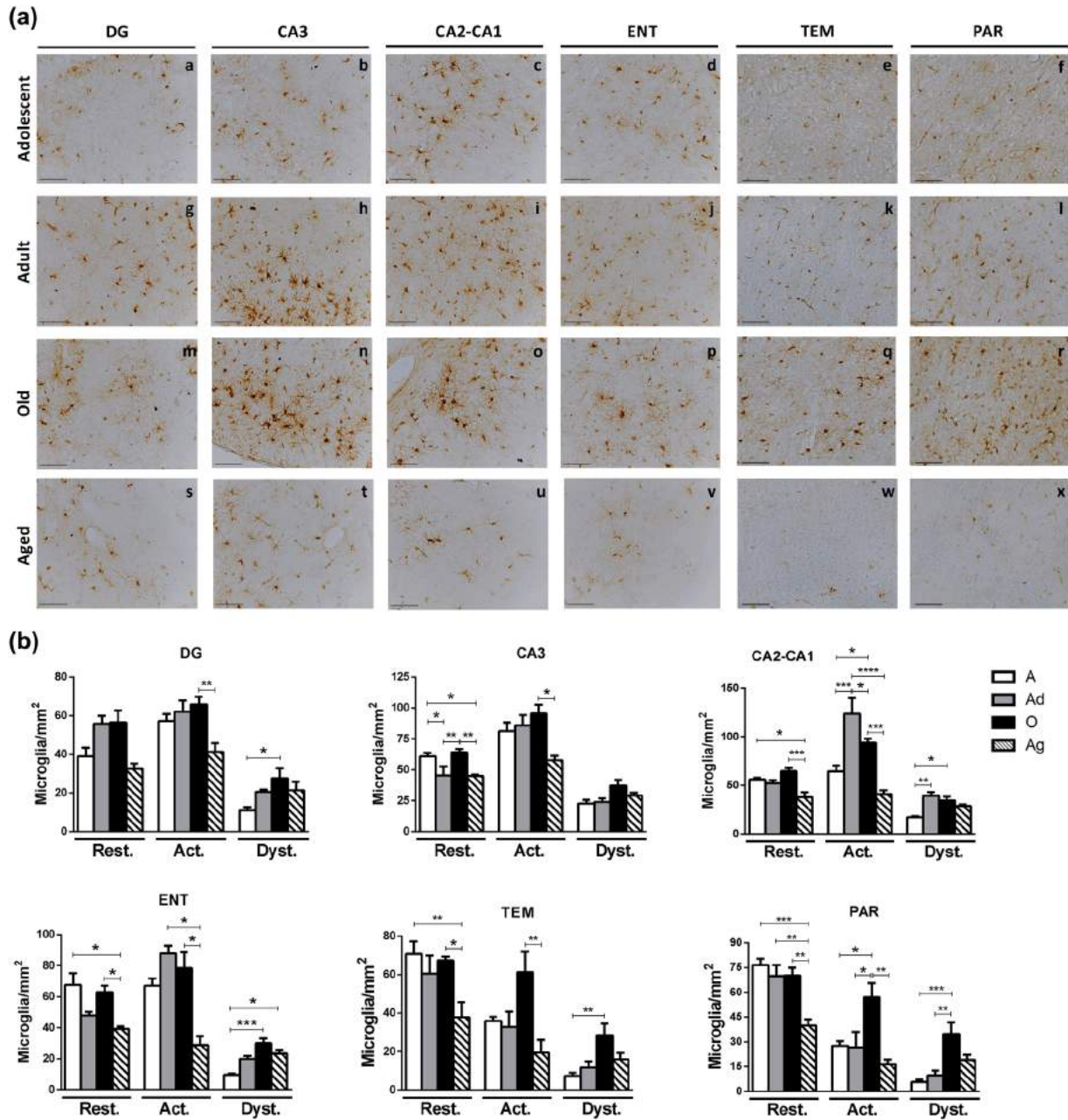
FIGURE 3 (a) Representative photomicrographs of ferritin+ cells in marmoset brain. Ferritin+ microglia was quantified in dentate gyrus (DG), hippocampal region (CA3 and CA2-CA1), entorhinal (ENT), temporal (TEM) and parietal (PAR) cortices of marmoset at different ages. Scale bar 200 μm. (b) Quantification of ferritin+ microglial by phenotype. Ferritin+ cells with microglia phenotype (resting -rest-, activated -act-, and dystrophic -dyst-) were quantified in different brain regions. Adolescent (A): mean age 1.75 ± 0.18 years; Adult (Ad): mean age 5.33 ± 0.88 years; Old (O): mean age 11.25 ± 0.7 years; Aged (Ag): mean age 16.83 ± 2.59 years. Data represents means ± S.E.M. One-way ANOVA followed by Tukey post hoc analysis. *$p < 0.05$; **$p < 0.01$; ***$p < 0.001$; ****$p < 0.0001$. See Table 1 for statistical differences

study, we reported that resting and activated microglia labeled with Iba1 in hippocampus of marmosets tend to decrease with age, while dystrophic microglia increases in aged individuals (Rodriguez-Callejas et al., 2016). In the present study we tested whether ferritin and Iba1 label the same microglia population in marmoset brains. We compared the data from the present study with data from our previous report (Rodriguez-Callejas et al., 2016), using the same brain regions and animals (Supplementary Figure S1b). Although both antibodies are

detected in same cytoplasmic compartment of microglia (Supplementary Figure S2), there were differences in their phenotype. While Iba1 tends to label preferentially resting microglia (adolescent and adult marmosets present more Iba1+ resting microglia, than ferritin+ resting microglia), ferritin preferentially labels activated microglia in all ages (Supplementary Figure S1b). Regarding dystrophic microglia, both antibodies labeled the same number of dystrophic cells in all regions and ages analyzed, except in aged marmoset where a slight decreased

TABLE 1 Densities of ferritin+ microglial phenotype in marmoset brain

	Adolescent	Adult	Old	Aged
Resting microglia/mm^2				
Dentate gyrus	39.13 ± 4.358	55.86 ± 4.197	56.50 ± 6.277	32.61 ± 2.615
CA3	61.06 ± 2.643[*,&]	45.42 ± 7.338[##]	64.21 ± 2.768[&&]	45.08 ± 1.073
CA2-CA1	56.10 ± 1.798[&]	52.23 ± 3.152	64.75 ± 3.716[&&&]	38.12 ± 4.944
Entorhinal cortex	67.81 ± 7.375[&]	48.01 ± 2.278	63.02 ± 4.302[&]	39.35 ± 1.562
Temporal cortex	70.75 ± 6.620[&&]	60.59 ± 9.331	67.43 ± 1.988[&]	37.89 ± 7.833
Parietal cortex	76.59 ± 3.930[&&&]	69.85 ± 6.773[&&]	70.35 ± 4.680[&&]	40.01 ± 3.678
Activated microglia/mm^2				
Dentate gyrus	57.25 ± 3.639	62.20 ± 5.758	65.87 ± 3.931[&&]	41.37 ± 4.509
CA3	81.43 ± 6.890	85.84 ± 8.466	95.64 ± 7.159[&]	57.80 ± 3.605
CA2-CA1	64.73 ± 5.873[***,#]	124.10 ± 16.210[#,&&&&]	93.89 ± 4.238[&&&]	41.16 ± 3.898
Entorhinal cortex	67.27 ± 4.715	88.06 ± 4.957[&]	78.55 ± 10.300[&]	28.99 ± 5.533
Temporal cortex	36.03 ± 2.061	32.91 ± 7.927	61.29 ± 10.730[&&]	19.47 ± 6.649
Parietal cortex	27.66 ± 2.873[#]	26.72 ± 9.427[#]	57.27 ± 8.461[&&]	16.46 ± 2.848
Dystrophic microglia/mm^2				
Dentate gyrus	11.17 ± 1.580[#]	20.61 ± 1.190	27.69 ± 5.188	21.44 ± 4.386
CA3	22.79 ± 2.958	24.06 ± 3.070	37.33 ± 4.579	29.29 ± 2.215
CA2-CA1	17.27 ± 1.205[**,#]	39.55 ± 3.710	34.55 ± 4.259	28.78 ± 1.522
Entorhinal cortex	9.66 ± 0.816[###,&]	20.03 ± 1.961	30.06 ± 3.135	23.45 ± 2.181
Temporal cortex	7.45 ± 1.509[##]	11.93 ± 2.993	28.58 ± 6.079	16.00 ± 3.357
Parietal cortex	5.84 ± 1.291[###]	9.81 ± 2.878[##]	34.82 ± 6.974	19.17 ± 3.217

Microglia phenotype data as represented in Figure 3. Data are summarized as Mean ± standard error of mean. *Significant difference against adult group; [#]significant differences against old group; [&]significant differences against aged group. One symbol: $p < 0.05$; two symbols: $p < 0.01$; three symbols: $p < 0.001$; four symbols: $p < 0.0001$.

in the number of ferritin+ dystrophic microglia was observed (Supplementary Figure S1b). Therefore, ferritin can be used as a marker to differentiate the phenotype of microglia, with a preference for activated microglia.

To assess if iron levels were related to the increased number of ferritin+ activated and dystrophic microglia during adulthood and aging, we performed a histochemical detection of iron in the same subjects.

3.2 | Increased iron tissue content and number of iron-storage microglia in hippocampus and cortex of aged marmosets

Iron labeling appeared mainly in the cytoplasm of different types of cell (Figure 4a, arrowheads). We quantified iron as a percentage of staining in a specific area and observed a significant increase in iron content in the hippocampus between old and aged marmosets. In the cortex, iron staining increased firstly between adult and old marmosets, and secondly between old and aged marmosets (Figure 4b, upper panel and Table 2). Then, the number of ferritin + microglia containing iron (microglia+ iron) was analyzed, and cells were identified with a dark-blue staining (Figure 4a, arrows).

Microglia+ iron density gradually increased along aging in all brain regions, being significantly higher in old individuals against adolescent ones. It then tends to decrease in aged marmosets (Figure 4b, lower panel and Table 2).

3.3 | Increased number of astrocytes in aged marmosets

Glial fibrillary acidic protein (GFAP) represents a specific marker for astrocytes, which are increased in normal aging (Cotrina & Nedergaard, 2002; Dong & Benveniste, 2001). Immunoreactivity for GFAP in hippocampus and entorhinal cortex of marmosets was detected and quantified (Figure 5a). Density of GFAP+ cells increased in aged marmoset compared to old and adult individuals in DG, while it increased in old subjects compared to younger animals in CA2-CA1 and ENT cortex (Figure 5b, upper panel). GFAP+ cell in ENT cortex decreased, though not significantly, in aged marmosets compared to old subjects (Figure 5b, upper panel). To explore whether these astrocytes showed hypertrophy, we assessed the relative soma size and found it to be increased during aging only in hippocampal regions (Figure 5b).
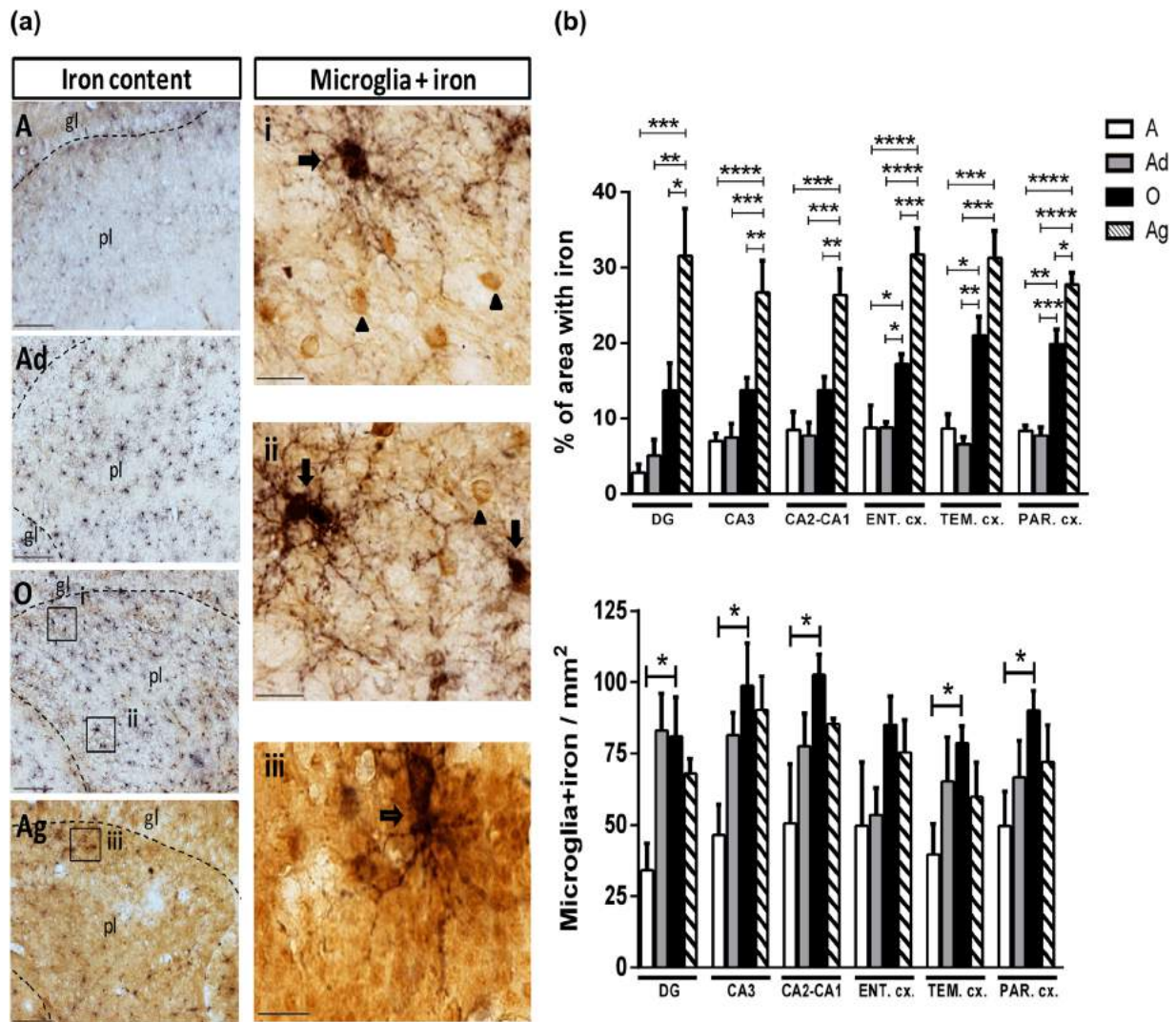
FIGURE 4 Detection of iron (histochemistry) and ferritin (immunohistochemistry) in hippocampus and cortex of marmosets. (a) Iron content (brown) and microglia labeled with iron (dark blue) were assessed in the hippocampus and cortex. Left: Representative images of iron content in the brain of marmoset at different ages. In hippocampus, there was a clear increase in iron tissue content with aging (brown color). Scale bar 100 μm. Right: Representative images of microglia+ iron (arrows). Note the presence of cells with low levels of iron but not ferritin (arrow heads) (inserts i and ii), and ferritin+ microglia with iron (microglia+iron) located in granular layer of DG (empty arrow) (insert iii) taken from left panels. Scale bar 20 μm. (b) Quantification of percentage area stained with iron, and density of microglia+ iron in adolescent (A), adult (Ad), old (O), and aged (Ag) marmosets. Upper panel: Iron content in hippocampal and cortical regions. Lower panel: Density of microglia + iron in hippocampal and cortical regions. Dentate gyrus (DG), Entorhinal (ENT), temporal (TEM), and parietal (PAR) cortices. Adolescent (A): mean age 1.75 ± 0.18 years; Adult (Ad): mean age 5.33 ± 0.88 years; Old (O): mean age 11.25 ± 0.7 years; Aged (Ag): mean age 16.83 ± 2.59 years. Data represents means ± S.E.M. One-way ANOVA followed by Tukey post hoc test. *$p < 0.05$; **$p < 0.01$; ***$p < 0.001$; ****$p < 0.0001$. See Table 2 for statistical differences

3.4 | RNA oxidation increases with aging in hippocampus and cortex of marmosets

The function of ferritin is to store iron inside cells to avoid Fenton reaction and subsequent free radical formation. As we observed an increase in the iron content in brain tissue during the aging process in marmosets, we sought to assess whether this increase in iron parallels cellular or physiological damage by oxidative stress. We evaluated a product of RNA oxidation, known as 8-hydroxyguanosine (8OHG) (Syslová et al., 2014), which was clearly identified allowing for its quantification in all regions of interest (Figure 6). In adolescent

marmosets, few cells are faintly labeled with 8OHG antibody in all hippocampal regions and cortices (Figure 6a–f). Adult, old, and aged marmosets showed a great increase in the amount of 8OHG+ cells, which appeared more intensively labeled than in adolescent subjects (Figure 6a, g–x). A high number of 8OHG+ cells were found in the granular and polymorphic layers of DG, and *stratum pyramidale* of CA3 and CA2-CA1. In TEM and PAR cortices, layers III, IV, and V were more intensely labeled than layers I and II, while ENT cortex exhibited a homogenous labeling of 8OHG (Figure 6a). It is important to note that in all hippocampal regions, 8OHG+ appeared mostly in cell cytoplasm

TABLE 2 Quantification of iron and microglia+ iron in marmoset brain

	Adolescent	Adult	Old	Aged
Percentage of area stained with iron (%)				
Dentate gyrus	$2.82 \pm 1.133^{\&\&\&}$	$5.10 \pm 2.092^{\&\&}$	$13.69 \pm 3.624^{\&}$	31.51 ± 6.298
CA3	$7.01 \pm 1.011^{\&\&\&\&}$	$7.47 \pm 1.819^{\&\&\&}$	$13.74 \pm 1.642^{\&\&}$	26.76 ± 4.135
CA2-CA1	$8.48 \pm 2.388^{\&\&\&}$	$7.72 \pm 1.693^{\&\&\&}$	$13.76 \pm 1.724^{\&\&}$	26.40 ± 3.390
Entorhinal cortex	$8.74 \pm 3.007^{\#,\&\&\&\&}$	$8.79 \pm 0.738^{\#,\&\&\&\&}$	$17.21 \pm 1.383^{\&\&\&}$	31.73 ± 3.434
Temporal cortex	$8.67 \pm 1.931^{\#,\&\&\&\&}$	$6.61 \pm 0.941^{\#\#,\&\&\&\&}$	21.03 ± 2.458	31.28 ± 3.584
Parietal cortex	$8.39 \pm 0.653^{\#\#,\&\&\&\&}$	$7.72 \pm 1.138^{\#\#,\&\&\&\&}$	$19.88 \pm 1.897^{\&}$	27.76 ± 1.521
Density of microglia+ iron/mm^2				
Dentate gyrus	$34.22 \pm 9.416^{\#}$	83.03 ± 13.150	81.05 ± 13.690	67.94 ± 5.202
CA3	$46.50 \pm 10.610^{\#}$	81.52 ± 7.958	98.83 ± 14.970	90.28 ± 11.890
CA2-CA1	$50.58 \pm 20.980^{\#}$	77.60 ± 11.570	102.80 ± 7.084	85.45 ± 1.994
Entorhinal cortex	49.82 ± 22.290	53.44 ± 9.502	85.08 ± 9.992	75.49 ± 11.430
Temporal cortex	$39.70 \pm 10.790^{\#}$	65.37 ± 15.510	78.70 ± 5.923	59.98 ± 12.000
Parietal cortex	$49.70 \pm 12.110^{\#}$	66.73 ± 12.850	90.04 ± 7.075	72.16 ± 12.930

Data are summarized as Mean ± standard deviation. [#]significant differences against old group; [&]significant differences against aged group. One symbol: $p < 0.05$; two symbols: $p < 0.01$; three symbols: $p < 0.001$; four symbols: $p < 0.0001$.

surrounding the nucleus. However, in the cortex of adult, old, and aged marmosets, 8OHG also appeared in neuronal dendrites (Figure 6a, l, r). The quantification of the percentage of area occupied by 8OHG+ cells, confirmed an increased RNA oxidation with age, since adult marmosets showed a significant increase in 8OHG+ cells compared to adolescent animals in CA3 and all cortical regions (Figure 6b and Table 3). Similarly, 8OHG+ cell density increased further with aging as all hippocampal and cortical regions showed a higher 8OHG staining in old and aged marmosets with respect to the adolescent group (Figure 6B and Table 3). Notably, in the cortical regions, 8OHG is greatly increased and remains stable in the three adult groups (Ad, O, Ag) compared to the adolescent (A) group. In hippocampal regions, 8OHG increased more progressively from A to Ag marmosets (Table 3). After gathering the data, we can conclude that RNA oxidation appears early in adulthood in both cortex and hippocampus of marmoset brains.

3.5 | RNA oxidation is present in neurons and astrocytes, but rarely in microglia.

We have observed a decrease in the density of resting and activated microglia but an increased number of cells showing RNA oxidation in aged marmoset brain. As RNA oxidation can lead to apoptosis (Shan, Chang, & Lin, 2007) and to reduction in cell number, we aimed to evaluate whether glia cells were suffering RNA oxidation, as it has been previously described in neurons (Ding, Markesbery, Cecarini, & Keller, 2006; Ding, Markesbery, Chen, Li, & Keller, 2005; Nunomura et al., 1999, 2001, 2002; Nunomura, Tamaoki et al., 2012). Double labeling immunofluorescence was performed in hippocampus of old and aged marmosets, using ferritin, Iba1, GFAP, and 8OHG antibodies. We were able to observe that astrocytes were positively co-labeled with 8OHG

(Supplementary Figure S3). These 8OHG+ astrocytes were mainly found in stratum radiatum of CA3 and CA2-CA1, in old and aged marmosets (Supplementary Figure S3). Double labeling of microglia and 8OHG resulted in a robust immunoreactivity of 8OHG in neuronal-like cells in pyramidal and granular layers of the hippocampus in old and aged marmosets. However, we did not detect significant 8OHG labeling in microglia (Figure 7). Notably, microglia were nearby 8OHG+ cells: their processes were surrounding damaged cells, as in a phagocytic phase (Figure 7 panel Q). We then quantified the number of microglia showing ramified processes or amoeboid morphology in hippocampus of old marmoset (Figure 7, yellow and white arrow). The amoeboid phenotype was more abundant than the ramified one (Figure 7 graph). Few microglia had positive staining for 8OHG throughout their cytoplasm, mainly in aged marmosets. We noted that those 8OHG+ microglia presented a few deramified processes, which could suggest a dystrophic phenotype (Figure 7, r panel, arrow head).

3.6 | Some M2 microglia showed a dystrophic phenotype

We observed activated microglia surrounding 8OHG+ *damaged* cells, resembling a M2 state (Jimenez et al., 2008; Tang & Le, 2016). Therefore, we aimed to determine if those microglia were in a phagocytic M2 state, which has been shown to express Arg1 and IL-10 (Cherry, Olschowka, & O'Banion, 2014; Cherry et al., 2015). Therefore, we performed double (IL-10 and ferritin), and triple (Arg1, ferritin, and 8OHG) immunofluorescence labeling and evaluated the presence of M2 microglia in the hippocampus of old marmosets (Figure 8). Most ferritin+ microglia showing a hypertrophic cytoplasm were positive for IL-10 and Arg1, characteristic of M2 state (Figure 8). Phagocytic

(a) GFAP + cells in different regions of the brain
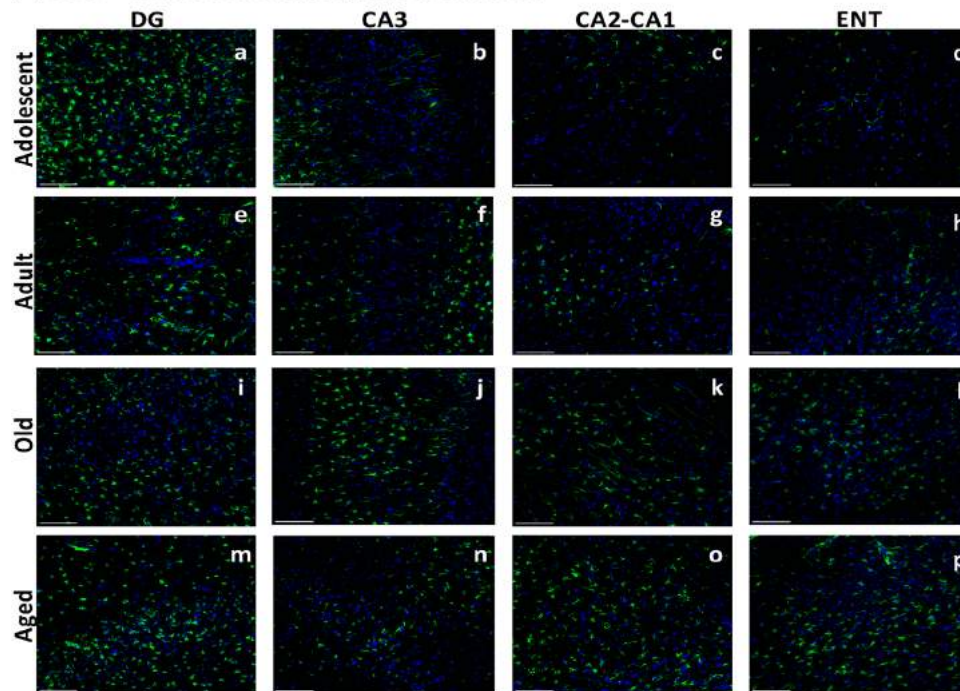
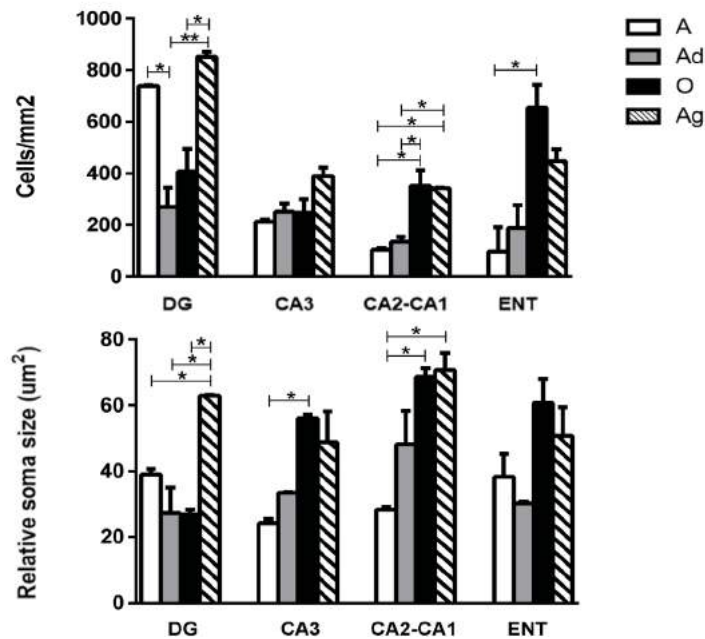## (b) Quantification of reactive astrocytes in brain of marmoset

FIGURE 5 Astrocytes labeled with GFAP. (a) Immunofluorescence of GFAP in different regions of the brain of adolescent (A) (a-d), adult (Ad) (e-h), old (O) (i-l), and aged (Ag) (m-p) marmosets. Scale bar 100 μm. (b) Quantification of GFAP+ cells (cells/mm^2) and their relative soma sizes in the respective regions analyzed. Upper panel: There was a significant increase in GFAP+ cells in O and Ag individuals compared to Ad in DG and CA2-CA1, and from A to Ag in CA2-CA1 and ENT (all, $p < 0.05$). Notably, A subjects presented a larger number of GFAP+ cells in DG compared to Ad ($p < 0.05$). Lower panel: Relative GFAP+ cells soma size was compared among age groups. It increased in Ag marmoset in DG and CA2-CA1 compared to younger subjects. In CA3 and CA2-CA1 regions, GFAP+ soma size increased already in O marmoset compared to Ad subjects. Adolescent (A): mean age 1.75 ± 0.18 years; Adult (Ad): mean age 5.33 ± 0.88 years; Old (O): mean age 11.25 ± 0.7 years; Aged (Ag): mean age 16.83$p < 2.59$ years. Data represents means ± S.E.M. One-way ANOVA post-hoc analysis Tukey (*$p < 0.01$, **$p < 0.01$)
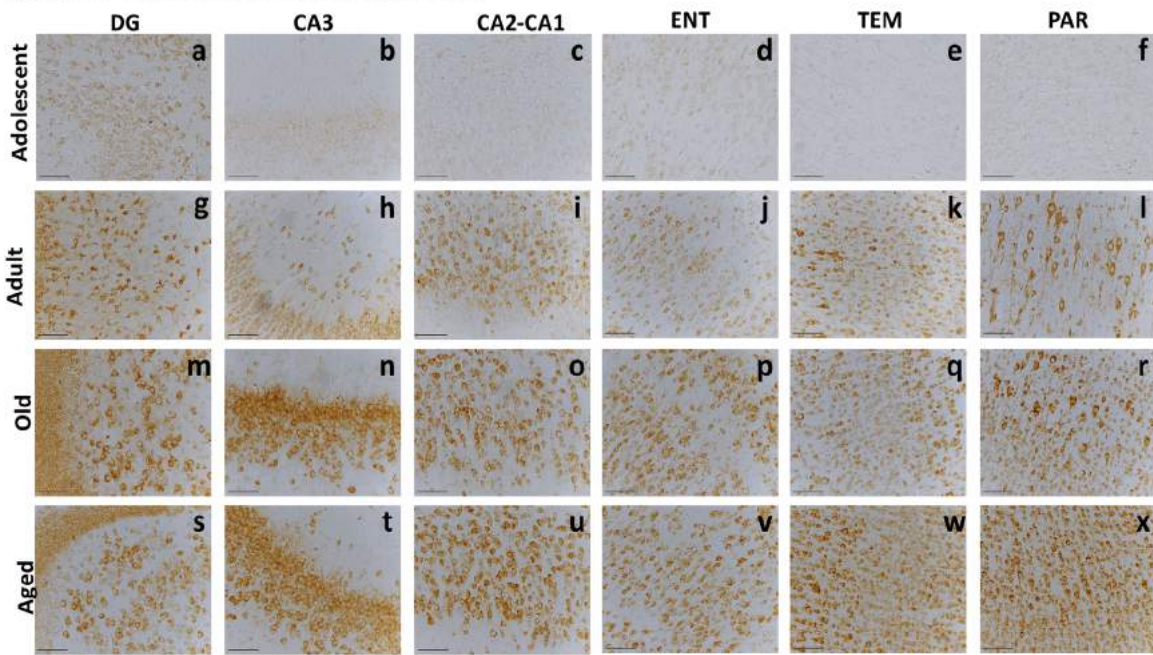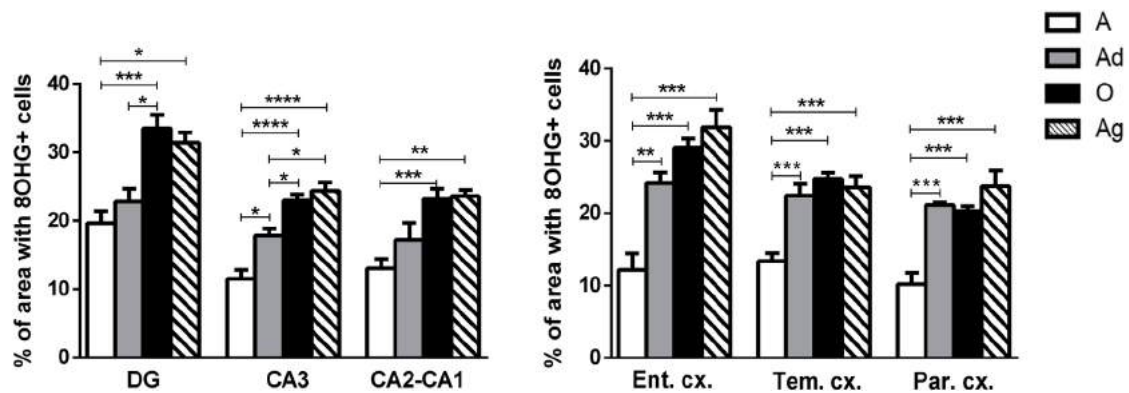
FIGURE 6 Immunohistochemistry for 8OHG in marmoset brain. (a) 8OHG labeling in hippocampus and cortex of marmoset. Oxidized RNA could be detected in adolescent marmoset brain (a-f), and it increased with aging. Adults showed an increased 8OHG labeling in all regions analyzed (g-l), with remarkable staining in parietal cortex (PAR) where large neurons can be detected (l). In old and aged marmosets, labeling was observed in all regions analyzed (m-x), being greater in DG's granule and polymorphic layers (m and s) and str. pyramidale from CA3 and CA2-CA1 (n, o, t, and u). Note, that large pyramidal neurons can be observed in PAR in adults but not in adolescent and aged marmosets (r and x). Scale bar 100 μm. (b) Percentage of area occupied by 8OHG+ cells. 8OHG+ cells increased along aging in all hippocampus and cortical regions, however, damage to RNA can be detected earlier in cortex than hippocampus. Adolescent (A): mean age 1.75 ± 0.18 years; Adult (Ad): mean age 5.33 ± 0.88 years; Old (O): mean age 11.25 ± 0.7 years; Aged (Ag): mean age 16.83 ± 2.59 years. Data represents means ± S.E.M. One-way ANOVA post hoc analysis Tukey. *$p < 0.05$; **$p < 0.01$; ***$p < 0.001$; ****$p < 0.0001$. See table 3 for statistical differences

spheroids were commonly labeled with Arg1 (Figure 8, white thick arrows). Triple immunofluorescence labeling with ferritin, Arg1, and 8OHG indicated that some microglia Arg1+ also had positive staining for 8OHG (Figure 8, middle panels, blue arrows). Moreover, we saw features of dystrophic phenotype on those M2 cells: phagocytic spheroids and cytoplasmic fragmentation (Hefendehl et al., 2014). Additionally, we also observed that ferritin+ intensity in those M2 dystrophic cells was much weaker than in M1 microglia (Figure 8, yellow arrows).

4 | DISCUSSION

4.1 | Activated microglia contains ferritin in brain of marmosets

We have shown that ferritin antibody allows a clear detection of microglia, labeling preferentially an activated phenotype (Figures 2, 3, and Supplementary Figure S1). Ferritin+ microglia were quantified according to the three main phenotypic types: resting, activated, and

TABLE 3 Percentage of area occupied by 8OHG+ cells in marmoset brain

	Adolescent (%)	Adult (%)	Old (%)	Aged (%)
Dentate gyrus	19.66 ± 1.778[###,&]	22.81 ± 1.885[#]	33.51 ± 2.008	31.45 ± 1.457
CA3	11.56 ± 1.287[*,####,&&&]	17.85 ± 0.988[#,&]	22.99 ± 0.875	24.41 ± 1.191
CA2-CA1	13.09 ± 1.344[###,&&]	17.20 ± 2.480	23.26 ± 1.425	23.62 ± 0.892
Entorhinal cortex	12.14 ± 2.260[**,###,&&&]	24.14 ± 1.476	29.07 ± 1.200	31.89 ± 2.382
Temporal cortex	13.34 ± 1.119[***,###,&&&]	22.41 ± 1.601	24.73 ± 0.814	23.55 ± 1.595
Parietal cortex	10.15 ± 1.571[***,###,&&&]	21.12 ± 0.319	20.27 ± 0.676	23.73 ± 2.150

Data are summarized as Mean ± standard deviation. Data are summarized as Mean ± standard deviation. *Mean significant difference against adult group; [#]represents significant differences against old group: [&]significant differences against aged group. One symbol: $p < 0.05$; two symbols: $p < 0.01$; three symbols: $p < 0.001$; four symbols: $p < 0.0001$.

dystrophic (Streit et al., 2004). Our data showed an increased number of ferritin+ microglia with activated and dystrophic phenotype in hippocampus and cortex from adult and old marmosets, compared to adolescent subjects. In contrast, the density of total ferritin+ microglia (resting, activated and dystrophic) decreased in aged marmosets (Figures 3 and Supplementary Figure S1). In the current study, we also compared ferritin labeling with Iba1 labeling (Ito et al., 1998) from our previous report (Rodriguez-Callejas et al., 2016). We observed that although both markers colocalize in the cytoplasmic domain of microglia (Supplementary Figure S2), ferritin labels preferentially activated microglia, whereas Iba1 labels rather resting cells in marmoset brains (Supplementary Figure S1). Ferritin, as a protein with ferroxidase activity, can store ferric ion for a long term (Arosio et al., 2009; Chasteen & Harrison, 1999), reducing reactive oxygen species (ROS) production. It was previously shown that the overexpression of the heavy subunit of ferritin in macrophages depends on the cytokines present in the environment and leads to polarization towards the M1 or M2 phenotype (Bolisetty et al., 2015). A similar observation was reported using antisera against the light subunit of ferritin, which preferentially label activated microglia (Kaneko, Kitamoto, Tateishi, & Yamaguchi, 1989). This data supports our current results as microglia positive for ferritin preferentially showed an activated phenotype in marmosets.

Previous work testing ferritin-, CD68-, Iba1-, and HLA-DR-immunoreactivity in brain samples from old healthy humans, or with dementia with Lewy bodies and AD (Lopes et al., 2008), have also observed a distinct population of microglia labeled with each antibody but conclude that ferritin preferentially labels dystrophic microglia in old and diseased patients (Lopes et al., 2008; Streit & Xue, 2016). Interestingly, when assessing ferritin+ microglia in healthy adult controls (aged 34–49 years of age), few ferritin+ cells could be detected, but the number of ferritin+ microglia increases in Down Syndrome patients (Xue & Streit, 2011). In the present study, we observed that number of ferritin+ cells was larger in adult and old marmosets compared to younger individuals in most brain regions analyzed. Hence, increased number of ferritin+ microglia in brain tissue may indicate the onset of aging or of a

disease condition similarly to human data (Lopes et al., 2008; Streit et al., 2009).

The increased density of ferritin+ microglia in old humans and in neurodegenerative diseases has been linked to the accumulation of iron. It has been proposed that dystrophy of microglia is the result of an impaired iron-mediated oxidative damage (Lopes et al., 2008; Streit & Xue, 2016). In this and in our previous study, we detected dystrophic microglia already in adolescent marmoset (Rodriguez-Callejas et al., 2016). Here we also observed a significant increase of 8OHG labelling since adulthood. This may indicate that in marmosets, the appearance of dysfunctional microglia parallels oxidative damage in the brain.

Importantly, iron concentration induces the expression of ferritin (Hare, Ayton, Bush, & Lei, 2013; Hentze, Muckenthaler, Galy, & Camaschella, 2010) and iron accumulation leads to increased ferritin immunoreactivity (Walker et al., 2016). This iron/ferritin balance is tightly regulated by the iron-responsive element binding proteins (IRP) that interacts with genes containing the iron responsive element (IRE). In contrast, ROS can oxidize ferritin by promoting its proteasomal degradation (Mehlhase, Sandig, Pantopoulos, & Grune, 2005), and ROS also inactivates c-aconitase, promoting inhibition of ferritin synthesis under IRP/IRE (Martins, Robalinho, & Meneghini, 1995; Pantopoulos & Hentze, 1995). The large number of cells showing oxidized RNA in old and aged marmosets may indicate an enhanced oxidative environment that may promote ferritin degradation and/or inhibit its synthesis by the above described mechanism. This was evident in aged marmoset, when the highest iron accumulation and RNA oxidation were present in the brain, but with a significant reduction of ferritin+ cells (resting, activated and dystrophic). Similarly, a dyshomeostasis between iron and ferritin levels has been observed in the substantia nigra of aged mouse (Walker et al., 2016). In AD patients, iron accumulates without a parallel increase in ferritin (Castellani et al., 2004) and a dysfunction of iron/ferritin system results in higher free iron levels in AD brain tissue (Bonda et al., 2011). Thus, increased iron/decreased ferritin ratio in aged marmoset may predispose brain tissue to oxidative damage and to neurodegeneration.
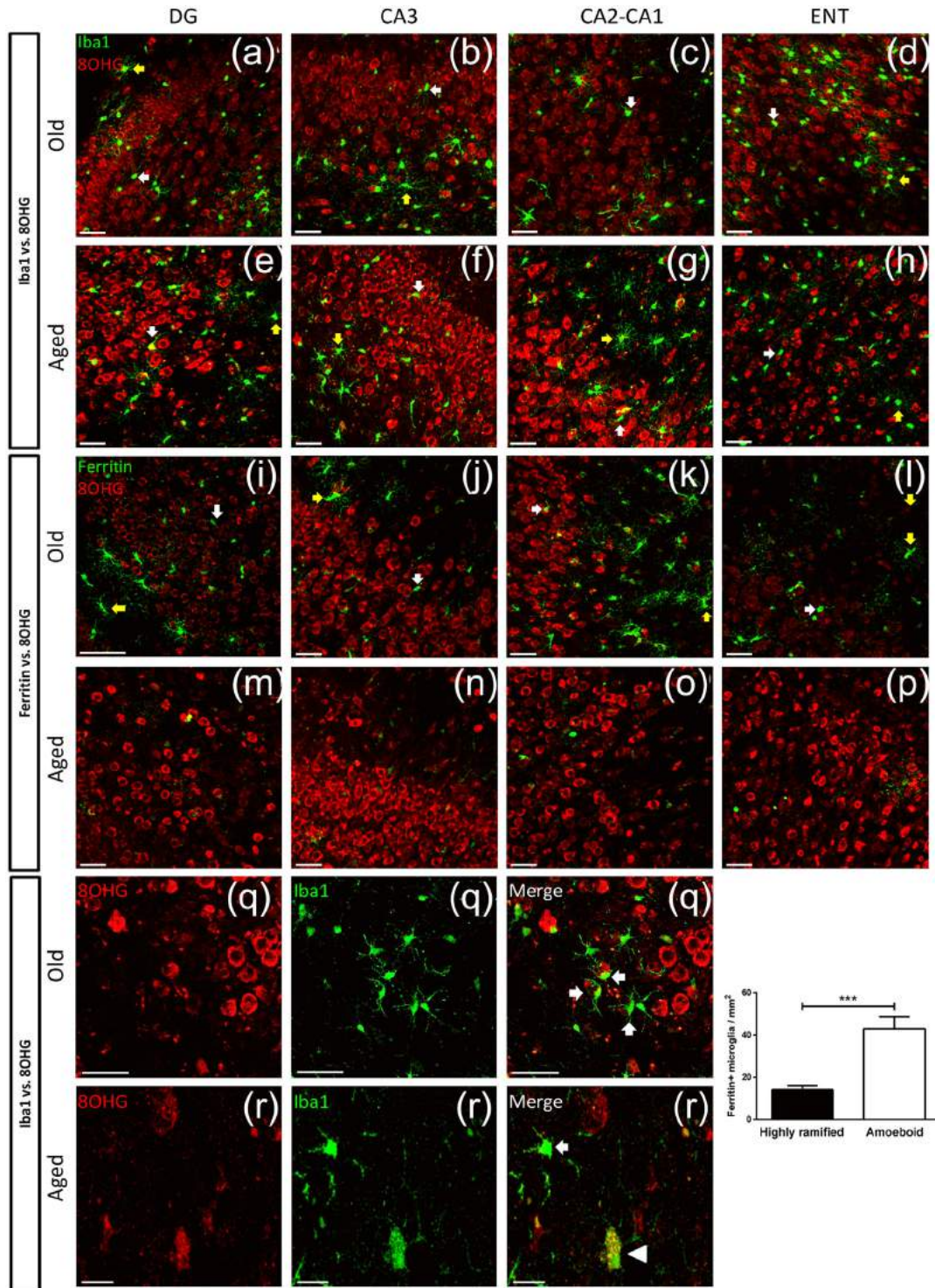
FIGURE 7 Double labeling of RNA oxidative stress marker 8OHG (red) and microglia (Iba1 or ferritin, green) in different hippocampal regions and entorhinal cortex (ENT). In all areas most of microglia (Iba1+ and ferritin+ cells) are not labeled with 8OHG, while some of them are surrounding 8OHG+ cells (f, g, q). Note that, as already shown in Figure 3 the number of ferritin+ microglia cells drastically decreased in aged marmosets (M-P). However, in aged marmosets Iba1+ microglia with few short deramified processes (such as in the dystrophic phenotype) were labeled with 8OHG throughout their cytoplasm (r, arrow head). Nearby, a microglia cell with activate phenotype was not 8OHG+ (r, arrow). (a–p) Scale bar 50 μm. (q, r) Scale bar 20 μm. Density of hypertrophic microglia in hippocampus of old marmoset. Ferritin+ microglia cells were scored as highly ramified microglia (hypertrophic soma with ramified processes, yellow arrows in panels (a–l) or amoeboid microglia (ameboid soma shape, white arrows in panels (a–l). Amoeboid microglia were more abundant than ramified microglia. Old (O): mean age 11.25 ± 0.7 years; Aged (Ag): mean age 16.83 ± 2.59 years. Data represents means ± S.E.M. Unpaired T-test (***$p < 0.001$)
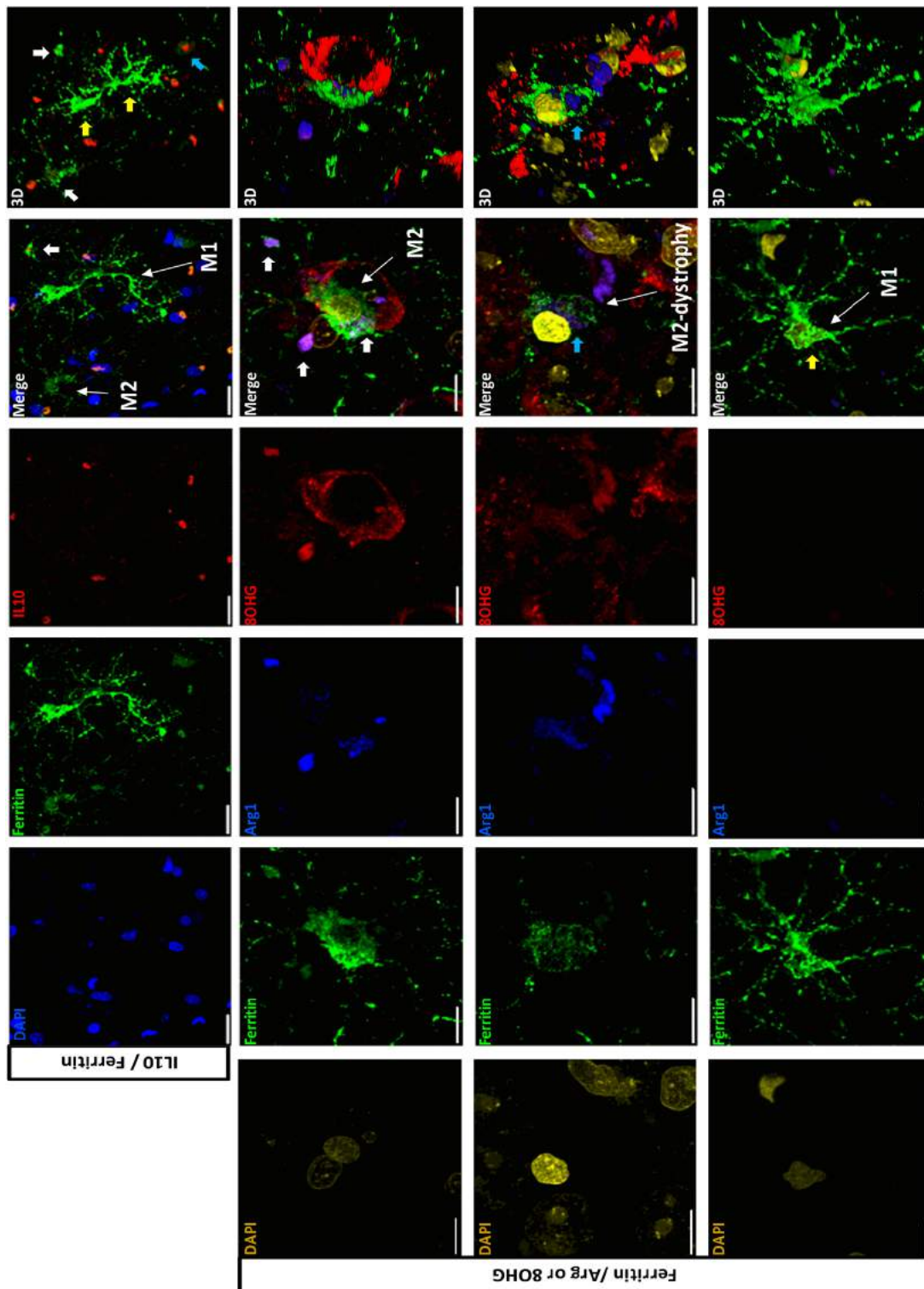
FIGURE 8 Ferritin + microglia cells are positive for interleukin 10 (IL10) and arginase 1 (Arg1) in hippocampus of old marmosets. Mean age of old marmoset was 11.25 ± 0.7 years. At the upper and bottom panels microglia (green) with a characteristic M1 state showing a hypertrophic cytoplasms and long ramified processes, but no labeling with either IL10 (red) or 8OHG (red) (yellow arrows). Middle panels: A triple labeling confirm that ferritin+ cells (green) co-localize with Arg1 (blue). This ferritin + microglia presented a hypertrophic soma and short processes and it was in close contact with 8OHG + cells located in granular layer (larger soma size). A three-dimensional reconstruction (last column), confirms the colocalization of Arg1 inside microglia, and its interaction with 8OHG+ cell, indicating a M2-phagocytic state (white arrows). Some ferritin + microglia with Arg1 immunoreactivity (M2 state) presented cytoplasmic 8OHG staining. Those microglia+ 8OHG were not surrounding damaged cells, but presented a dystrophic phenotype, such as a defragmented cytoplasm and de-ramified processes (blue arrows). Merge: surface rendering view using LSM software constructed from serial confocal z-stack images of each row. 3D: Three-dimensional reconstruction. Scale bar 20 μm (upper panel), 10 μm (rest of the panels)

4.2 | RNA oxidation increased in neurons and astrocytes, but microglia cells are protected from oxidative damage during aging, except some M2 type that showed a dystrophic phenotype

In the aging brain, as well as in several neurodegenerative diseases, there is a decline in the normal antioxidant defense mechanisms, which increases the vulnerability of the brain to the deleterious effects of oxidative damage (Finkel & Holbrook, 2000). Several studies have found increased levels of 8OHG in brain of old rats (Hamilton et al., 2001), as well as in hippocampus, TEM lobe, and inferior PAR lobe of old humans (Ding et al., 2006, 2005, Nunomura et al., 1999, 2001, 2002; Nunomura, Tamaoki et al., 2012). In marmosets, we observed an age-dependent increase in the number of 8OHG+ cells from adult to aged subjects. 8OHG labeled neuron like-cells and star-shaped cells resembling astrocytes. Double labeling confirmed a great number of astrocytes (GFAP+) with 8OHG in hippocampus of aged subjects (Supplementary Figure S3). The number of GFAP+ cells increased with aging in hippocampus, but it decreased, though non-significant in ENT cortex. These results are supported by previous observations of an excessive astrocyte activation in hippocampus during the aging process, whereas astrocytes seem to be atrophic in ENT cortex (Rodríguez-Arellano, Parpura, Zorec, & Verkhratsky, 2016). As we have focused the present work on the description of aged microglia, we did not use other markers to detect dystrophic/atrophic astrocytes that can be result of oxidized RNA. Further studies are needed to determine whether oxidative damage may be linked to astrocyte reduction in ENT cortex in aged marmosets.

Contrastingly, most microglia (labeled with ferritin and Iba1-antibodies) were not positive for 8OHG. This negative labeling was observed in all regions analyzed, and at all ages studied. Interestingly, microglia negative for 8OHG were often surrounding 8OHG+ cells in granular and pyramidal layers of hippocampus. Microglia have several mechanism of protection against RNA oxidation, such as over-expression of glutathione (Chatterjee, Noack, Possel, Keilhoff, & Wolf, 1999), superoxide dismutase 2 (SOD-2) (Ishihara, Takemoto, Itoh, Ishida, & Yamazaki, 2015), and inflammation-related protein autotaxin (ATX) (Awada et al., 2012). Microglia also exhibit the highest activity of glutathione peroxidase among other cells within the central nervous system (Power & Blumbergs, 2009). However, during aging those neuroprotective mechanisms are diminished, leading to cellular degeneration (dystrophy).

As we observed that 8OHG+ cells were surrounded by microglia, as in a phagocytic phase, we sought to quantify the number of hypertrophic activated microglia either with ramified processes or with an amoeboid soma. We found a higher number of amoeboid than ramified microglia in the dentate gyrus of old marmosets. We then detected ferritin+ microglia with markers of M2 state (Arg1 and IL10) (Cameron & Landreth, 2010; Franco & Fernández-Suárez, 2015; Kabba et al., 2017; Orihuela, McPherson, & Harry, 2016; Tang & Le, 2016). Those M2 microglia were surrounding and contacting other cells affected with RNA oxidation (8OHG+ cells, Figure 8), resembling a phagocytic process. Phagocytosis is a process that requires the

production of high levels of ROS (Splettstoesser & Schuff-Werner, 2002; Vernon & Tang, 2013) and eventually oxidative damage. In the present study, we observed that some M2 microglia had RNA oxidation and cytorrhexis (feature of dystrophy). An increased number of microglia with heterogeneous intracellular inclusions has been described in old rhesus monkeys (25–35 years). However, those microglia showed a reduced capacity to digest engulfed particles (Peters, Josephson, & Vincent, 1991). It has been proposed that reduced clearance of phagocytic debris in aged microglia may contribute to the onset of dystrophy (Spittau, 2017; von Bernhardi et al., 2015). In addition, during aging, autophagy efficiency declines and becomes dysfunctional, resulting in the accumulation of waste materials within cells (Salminen, Kaarniranta, & Kauppinen, 2012). Hence, previous studies and our current data may suggest that M2 microglia from aged marmoset, with a reduced antioxidant defense mechanism, may be more vulnerable to the production of ROS during phagocytosis causing oxidized RNA. Furthermore, a major consequence of this impaired phagocytic function is the aggregation of abnormal proteins, as we previously showed in aged marmoset, where dystrophic microglia accumulates hyperphosphorylated tau (Rodriguez-Callejas et al., 2016). Thus, M2 microglia that accumulates waste materials and present RNA oxidation in old and aged marmosets may become dysfunctional over the time (dystrophic), leaving brain tissue without a key defense and repair mechanisms, which may compromise brain functions.

Female marmosets showed impairments in cognitive flexibility compared to age-matched males (Workman, Healey, Carlotto, & Lacreuse, 2018). Moreover, sex differences in distractibility and motivation during cognitive task are exacerbated over time (Sadoun, Strelnikov, Bonté, Fonta, & Girard, 2015). It is known that in AD, women are in higher risk to develop the disease than men (Nebel et al., 2018), and female AD transgenic mice have more severe pathology compared to males (Clinton et al., 2007; Schäfer, Wirths, Multhaup, & Bayer, 2007; Wang, Tanila, Puoliväli, Kadish, & Van Groen, 2003). In this study we used brains of male marmosets. However, based on our current findings and on previous reports, it will be interesting to evaluate if the onset of microglia dystrophy, iron/ferritin disbalance and oxidative stress is enhanced in female marmosets' brains compared to males.

Early reports showed that executive functions are impaired in old non-human primates compared to young subjects (Lai, Moss, Killiany, Rosene, & Herndon, 1995; Moore, Killiany, Herndon, Rosene, & Moss, 2003). However, learning impairments in tasks, such as reversal learning and delayed matching-to-position can be detected even in young-adult marmosets (4 years of age) (Sadoun, Rosito, Fonta, & Girard, 2018). We also observed several brain alterations that are characteristic of aging or neurodegenerative conditions in marmosets starting in adulthood, such as dystrophic microglia, tau hyperphosphorylation, and increased RNA oxidation. Hence, marmosets seem to be a non-human primate with early onset of brain aging.

In this study we demonstrated that iron/ferritin ratio is imbalanced in the brains of aged marmoset, an event related to RNA oxidation and microglia dystrophy. Furthermore, adult marmosets present early

cellular and biochemical abnormalities related to aging and neuro-degeneration. Therefore, marmosets can be positioned as an ideal animal model to explore the pathological process of an accelerated brain aging and neurodegeneration.

ORCID

Claudia Perez-Cruz iD http://orcid.org/0000-0002-5983-307X

REFERENCES

Abbott, D., & Barnett, D. (2003). Aspects of common marmoset basic biology and life history important for biomedical research. *Comparative Medicine*, *53*(4), 339–350.

Arosio, P., Ingrassia, R., & Cavadini, P. (2009). Ferritins: A family of molecules for iron storage, antioxidation and more. *Biochimica Et Biophysica Acta – General Subjects*, *1790*(7), 589–599. http://doi.org/10.1016/j.bbagen.2008.09.004.

Awada, R., Rondeau, P., Grès, S., Saulnier-Blache, J. S., Lefebvre D'Hellencourt, C., & Bourdon, E. (2012). Autotaxin protects microglial cells against oxidative stress. *Free Radical Biology and Medicine*, *52*(2), 516–526. http://doi.org/10.1016/j.freeradbiomed.2011.11.014.

Balla, G., Jacob, H. S., Balla, J., Rosenberg, M., Nath, K., Apple, F., . . . Vercellotti, G. M. (1992). Ferritin: A cytoprotective antioxidant strategem of endothelium. *Journal of Biological Chemistry*, *267*(25), 18148–18153.

Bolisetty, S., Zarjou, A., Hull, T. D., Traylor, A., Joseph, R., Kamal, A. I., . . . Academy, H. (2015). Macrophage and epithelial cell H-ferritin expression regulates renal inflammation. *Kidney International*, *88*(1), 95–108. http://doi.org/10.1038/ki.2015.102.Macrophage.

Bonda, D. J., Lee, H., Blair, J. A., Zhu, X., Perry, G., & Smith, M. A. (2011). Role of metal dyshomeostasis in Alzheimer's disease. *Metallomics*, *3*(3), 267–270. http://doi.org/10.1039/C0MT00074D.

Braak, H., Alafuzoff, I., Arzberger, T., Kretzschmar, H., & Tredici, K. (2006). Staging of Alzheimer disease-associated neurofibrillary pathology using paraffin sections and immunocytochemistry. *Acta Neuropathologica*, *112*(4), 389–404. http://doi.org/10.1007/s00401-006-0127-z.

Braak, H., & Braak, E. (1991). Neuropathological stageing of Alzheimer-related changes. *Acta Neuropathologica*, *82*(4), 239–259.

Braak, H., & Braak, E. (1995). Staging of alzheimer's disease-related neurofibrillary changes. *Neurobiology of Aging*, *16*(3), 271–278. http://doi.org/10.1016/0197-4580(95)00021-6.

Cameron, B., & Landreth, G. E. (2010). Inflammation, microglia, and Alzheimer's disease. *Neurobiology of Disease*, *37*(3), 503–509. http://doi.org/10.1016/j.nbd.2009.10.006.

Castellani, R. J., Honda, K., Zhu, X., Cash, A. D., Nunomura, A., Perry, G., & Smith, M. A. (2004). Contribution of redox-active iron and copper to oxidative damage in Alzheimer disease. *Ageing Research Reviews*, *3*(3), 319–326. http://doi.org/10.1016/j.arr.2004.01.002.

Cermak, J., Balla, J., Jacob, H. S., Balla, G., Enright, H., Nath, K., & Vercellotti, G. M. (1993). Tumor cell heme uptake induces ferritin synthesis resulting in altered oxidant sensitivity: Possible role in chemotherapy efficacy. *Cancer Research*, *53*(21), 5308–5313.

Chang, Y., Kong, Q., Shan, X., Tian, G., Ilieva, H., Cleveland, D. W., . . . Lin, C. L. G. (2008). Messenger RNA oxidation occurs early in disease

pathogenesis and promotes motor neuron degeneration in ALS. *PLoS ONE*, *3*(8), e2849. http://doi.org/10.1371/journal.pone.0002849.

Chasteen, N. D., & Harrison, P. M. (1999). Mineralization in ferritin: An efficient means of iron storage. *Journal of Structural Biology*, *126*(3), 182–194. http://doi.org/10.1006/jsbi.1999.4118.

Chatterjee, S., Noack, H., Possel, H., Keilhoff, G., & Wolf, G. (1999). Glutathione levels in primary glial cultures: Monochlorobimane provides evidence of cell type-specific distribution. *Glia*, *27*(2), 152–161. http://doi.org/10.1002/(SICI)1098-1136(199908)27:2<152::AID-GLIA5>3.0.CO;2-Q.

Che, Y., Wang, J. F., Shao, L., & Young, L. T. (2010). Oxidative damage to RNA but not DNA in the hippocampus of patients with major mental illness. *Journal of Psychiatry and Neuroscience*, *35*(5), 296–302. http://doi.org/10.1503/jpn.090083.

Cherry, J. D., Olschowka, J. A., & O'Banion, M. K. (2014). Neuro-inflammation and M2 microglia: The good, the bad, and the inflamed. *Journal of Neuroinflammation*, *11*, 1–15. http://doi.org/10.1186/1742-2094-11-98.

Cherry, J. D., Olschowka, J. A., & O'Banion, M. K. (2015). Arginase 1+ microglia reduce Aβ plaque deposition during IL-1β-dependent neuro-inflammation. *Journal of Neuroinflammation*, *12*(1), 1–13. http://doi.org/10.1186/s12974-015-0411-8.

Clinton, L. K., Billings, L. M., Green, K. N., Caccamo, A., Ngo, J., Oddo, S., . . . LaFerla, F. M. (2007). Age-dependent sexual dimorphism in cognition and stress response in the 3xTg-AD mice. *Neurobiology of Disease*, *28*(1), 76–82. http://doi.org/10.1016/j.nbd.2007.06.013.

Cotrina, M. L., & Nedergaard, M. (2002). Astrocytes in the aging brain. *Journal of Neuroscience Research*, *67*(1), 1–10. http://doi.org/10.1002/jnr.10121.

Ding, Q., Markesbery, W. R., Cecarini, V., & Keller, J. N. (2006). Decreased RNA, and increased RNA oxidation, in ribosomes from early Alzheimer's disease. *Neurochemical Research*, *31*(5), 705–710. http://doi.org/10.1007/s11064-006-9071-5.

Ding, Q., Markesbery, W. R., Chen, Q., Li, F., & Keller, J. N. (2005). Ribosome dysfunction is an early event in Alzheimer's Disease. *Journal of Neuroscience*, *25*(40), 9171–9175. http://doi.org/10.1523/JNEUROSCI. 3040–05.2005.

Dong, Y., & Benveniste, E. N. (2001). Immune function of astrocytes. *Glia*, *36*(2), 180–190. http://doi.org/10.1002/glia.1107.

Finkel, T., & Holbrook, N. J. (2000). Oxidants, oxidative stress and the biology of ageing. *Nature*, *408*(6809), 239–247. http://doi.org/10.1038/35041687.

Franco, R., & Fernández-Suárez, D. (2015). Alternatively activated microglia and macrophages in the central nervous system. *Progress in Neurobiology*, *131*, 65–86. http://doi.org/10.1016/j.pneurobio.2015.05.003.

Guan, H., Yang, H., Yang, M., Yanagisawa, D., Bellier, J. P., Mori, M., . . . Tooyama, I. (2017). Mitochondrial ferritin protects SH-SY5Y cells against H2O2-induced oxidative stress and modulates α-synuclein expression. *Experimental Neurology*, *291*, 51–61. http://doi.org/10.1016/j.expneurol.2017.02.001.

Hamilton, M. L., Van Remmen, H., Drake, J. A., Yang, H., Guo, Z. M., Kewitt, K., . . . Richardson, A. (2001). Does oxidative damage to DNA increase with age?. *Proceedings of the National Academy of Sciences of the United States of America*, *98*(18), 10469–10474. http://doi.org/10.1073/pnas.171202698.

Hanisch, U.-K. K., & Kettenmann, H. (2007). Microglia: Active sensor and versatile effector cells in the normal and pathologic brain. *Nature Neuroscience*, *10*(11), 1387–1394. http://doi.org/10.1038/nn1997.

Hare, D., Ayton, S., Bush, A., & Lei, P. (2013). A delicate balance: Iron metabolism and diseases of the brain. *Frontiers in Aging Neuroscience*, *5*(34), 1–19. http://doi.org/10.3389/fnagi.2013.00034.

Hart, A. D., Wyttenbach, A., Hugh Perry, V., & Teeling, J. L. (2012). Age related changes in microglial phenotype vary between CNS regions: Grey versus white matter differences. *Brain, Behavior, and Immunity*, *26*(5), 754–765. http://doi.org/10.1016/j.bbi.2011.11.006.

Hefendehl, J. K., Neher, J. J., Sühs, R. B., Kohsaka, S., Skodras, A., & Jucker, M. (2014). Homeostatic and injury-induced microglia behavior in the aging brain. *Aging Cell*, 13(1), 60–69. http://doi.org/10.1111/acel.12149.

Hentze, M. W., Muckenthaler, M. U., Galy, B., & Camaschella, C. (2010). Two to tango: Regulation of mammalian iron metabolism. *Cell*, 142(1), 24–38. http://doi.org/10.1016/j.cell.2010.06.028.

Imai, Y., Ibata, I., Ito, D., Ohsawa, K., & Kohsaka, S. (1996). A novel gene iba1 in the major histocompatibility complex class III region encoding an EF hand protein expressed in a monocytic lineage. *Biochemical and Biophysical Research Communications*, 224(3), 855–862. http://doi.org/10.1006/bbrc.1996.1112.

Ishihara, Y., Takemoto, T., Itoh, K., Ishida, A., & Yamazaki, T. (2015). Dual role of superoxide dismutase 2 induced in activated microglia: Oxidative stress tolerance and convergence of inflammatory responses. *Journal of Biological Chemistry*, 290(37), 22805–22817. http://doi.org/10.1074/jbc.M115.659151.

Ito, D., Imai, Y., Ohsawa, K., Nakajima, K., Fukuuchi, Y., & Kohsaka, S. (1998). Microglia-specific localisation of a novel calcium binding protein, Iba1. *Molecular Brain Research*, 57(1), 1–9. http://doi.org/10.1016/S0169-328X(98)00040-0.

Jimenez, S., Baglietto-Vargas, D., Caballero, C., Moreno-Gonzalez, I., Torres, M., Sanchez-Varo, R., . . . Vitorica, J. (2008). Inflammatory response in the hippocampus of PS1M146L/APP751SL mouse model of Alzheimer's Disease: Age-dependent switch in the microglial phenotype from alternative to classic. *Journal of Neuroscience*, 28(45), 11650–11661. http://doi.org/10.1523/JNEUROSCI. 3024–08.2008.

Kabba, J. A., Xu, Y., Christian, H., Ruan, W., Chenai, K., Xiang, Y., . . . Pang, T. (2018). Microglia: Housekeeper of the central nervous system. *Cellular and Molecular Neurobiology*, 38(1), 53–71. http://doi.org/10.1007/s10571-017-0504-2.

Kaneko, Y., Kitamoto, T., Tateishi, J., & Yamaguchi, K. (1989). Ferritin immunohistochemistry as a marker for microglia. *Acta Neuropathologica*, 79(2), 129–136. http://doi.org/10.1007/BF00294369.

Kettenmann, H., Hanisch, U.-K., Noda, M., & Verkhratsky, A. (2011). Physiology of microglia. *Physiological Reviews*, 91(2), 461–553. http://doi.org/10.1152/physrev.00011.2010.

Kong, Q., & Lin, C. L. G. (2010). Oxidative damage to RNA: Mechanisms, consequences, and diseases. *Cellular and Molecular Life Sciences*, 67(11), 1817–1829. http://doi.org/10.1007/s00018-010-0277-y.

Lai, Z. C., Moss, M. B., Killiany, R. J., Rosene, D. L., & Herndon, J. G. (1995). Executive system dysfunction in the aged monkey: Spatial and object reversal learning. *Neurobiology of Aging*, 16(6), 947–954. http://doi.org/10.1016/0197-4580(95)02014-4.

Lin, F., & Girotti, A. W. (1998). Hemin-enhanced resistance of human leukemia cells to oxidative killing: Antisense determination of ferritin involvement. *Archives of Biochemistry and Biophysics*, 352(1), 51–58. http://doi.org/10.1006/abbi.1998.0588.

Lopes, K. O., Sparks, D. L., & Streit, W. J. (2008). Microglial dystrophy in the aged and Alzheimer's disease brain is associated with ferritin immunoreactivity. *Glia*, 56(10), 1048–1060. http://doi.org/10.1002/glia.20678.

Martins, E. A. L., Robalinho, R. L., & Meneghini, R. (1995). Oxidative stress induces activation of cytosolic protein responsible for control of iron uptake. *Archives of Biochemistry and Biophysics*.

Mehlhase, J., Sandig, G., Pantopoulos, K., & Grune, T. (2005). Oxidation-induced ferritin turnover in microglial cells: Role of proteasome. *Free Radical Biology and Medicine*, 38(2), 276–285. http://doi.org/10.1016/j.freeradbiomed.2004.10.025.

Moehle, M. S., & West, A. B. (2015). M1 and M2 immune activation in Parkinson's Disease: Foe and ally? *Neuroscience*, 302, 59–73. http://doi.org/10.1016/j.neuroscience.2014.11.018.

Moore, T. L., Killiany, R. J., Herndon, J. G., Rosene, D. L., & Moss, M. B. (2003). Impairment in abstraction and set shifting in aged Rhesus monkeys. *Neurobiology of Aging*, 24(1), 125–134. http://doi.org/10.1016/S0197-4580(02)00054-4.

Moreno-Gonzalez, I., Baglietto-Vargas, D., Sanchez-Varo, R., Jimenez, S., Trujillo-Estrada, L., Sanchez-Mejias, E., . . . Gutierrez, A. (2009). Extracellular amyloid-β and cytotoxic glial activation induce significant entorhinal neuron loss in young PS1M146V/APP751SL mice. *Journal of Alzheimer's Disease*, 18(4), 755–776. http://doi.org/10.3233/JAD-2009-1192.

Navarro, V., Sanchez-Mejias, E., Jimenez, S., Muñoz-Castro, C., Sanchez-Varo, R., Davila, J. C., . . . Vitorica, J. (2018). Microglia in Alzheimer's disease: Activated, dysfunctional or degenerative. *Frontiers in Aging Neuroscience*, 10(140), 1–8. http://doi.org/10.3389/fnagi.2018.00140.

Nebel, R. A., Aggarwal, N. T., Barnes, L. L., Gallagher, A., Goldstein, J. M., Kantarci, K., . . . Mielke, M. M. (2018). Understanding the impact of sex and gender in Alzheimer's disease: A call to action. *Alzheimer's & Dementia*, 14(9), 1–13. http://doi.org/10.1016/j.jalz.2018.04.008.

Nimmerjahn, A., Kirchhoff, F., & Helmchen, F. (2005). Resting microglial cells are highly dynamic surveillants of brain parenchyma in vivo. *Science*, 308(May), 1314–1319. http://doi.org/10.1126/science.1110647.

Nunomura, A., Chiba, S., Kosaka, K., Takeda, A., Castellani, R. J., Smith, M. A., & Perry, G. (2002). Neuronal RNA oxidation is a prominent feature of dementia with Lewy bodies. *Neuroreport*, 13(16), 2035–2039.

Nunomura, A., Moreira, P. I., Castellani, R. J., Lee, H. G., Zhu, X., Smith, M. A., & Perry, G. (2012). Oxidative damage to RNA in aging and neurodegenerative disorders. *Neurotoxicity Research*, 22(3), 231–248. http://doi.org/10.1007/s12640-012-9331-x.

Nunomura, A., Perry, G., Aliev, G., Hirai, K., Takeda, A., Balraj, E., . . . Smith, M. A. (2001). Oxidative damage is the earliest event in Alzheimer disease. *Journal of Neuropathology and Experimental Neurology*, 60(8), 759–767. http://doi.org/10.1093/jnen/60.8.759.

Nunomura, A., Perry, G., Pappolla, M. A., Wade, R., Hirai, K., Chiba, S., & Smith, M. A. (1999). RNA oxidation is a prominent feature of vulnerable neurons in Alzheimer's disease. *The Journal of Neuroscience*, 19(6), 1959–1964. http://doi.org/10.1523/JNEUROSCI.19-06-01959.

Nunomura, A., Tamaoki, T., Motohashi, N., Nakamura, M., McKeel, D. W., Tabaton, M., . . . Zhu, X. (2012). The earliest stage of cognitive impairment in transition from normal aging to Alzheimer Disease is marked by prominent RNA oxidation in vulnerable neurons. *Journal of Neuropathology & Experimental Neurology*, 71(3), 233–241. http://doi.org/10.1097/NEN.0b013e318248e614.

Orihuela, R., McPherson, C. A., & Harry, G. J. (2016). Microglial M1/M2 polarization and metabolic states. *British Journal of Pharmacology*, 173(4), 649–665. http://doi.org/10.1111/bph.13139.

Orino, K., Lehman, L., Tsuji, Y., Ayaki, H., Torti, S. V., & Torti, F. M. (2001). Ferritin and the response to oxidative stress. *Biochemical Journal*, 357(1), 241–247. http://doi.org/10.1042/bj3570241.

Pantopoulos, K., & Hentze, M. W. (1995). Rapid responses to oxidative stress mediated by iron regulatory protein. *The EMBO Journal*, 14(12), 2917–2924.

Paxinos G., Watson C., Petrides M., Rosa M., & Tokuno H. (2012). *The marmoset brain in stereotaxic coordinates* (1st ed.). San Diego, CA, USA: Elsevier Inc.

Peters, A., Josephson, K., & Vincent, S. L. (1991). Effects of aging on the neuroglial cells and pericytes within area 17 of the rhesus monkey cerebral cortex. *The Anatomical Record*, 229(3), 384–398. http://doi.org/10.1002/ar.1092290311.

Power, J. H. T., & Blumbergs, P. C. (2009). Cellular glutathione peroxidase in human brain: Cellular distribution, and its potential role in the degradation of Lewy bodies in Parkinson's disease and dementia with Lewy bodies. *Acta Neuropathologica*, 117, 63–73. http://doi.org/10.1007/s00401-008-0438-3.

Ramos, P., Santos, A., Pinto, N. R., Mendes, R., Magalhães, T., & Almeida, A. (2014). Iron levels in the human brain: A post-mortem study of anatomical region differences and age-related changes. *Journal of Trace Elements in Medicine and Biology*, 28(1), 13–17. http://doi.org/10.1016/j.jtemb.2013.08.001.

Ransohoff, R. M., & Perry, V. H. (2009). Microglial physiology: Unique stimuli, specialized responses. *Annual Review of Immunology*, *27*, 119–145. http://doi.org/10.1146/annurev.immunol.021908.132528.

Rodríguez-Arellano, J. J., Parpura, V., Zorec, R., & Verkhratsky, A. (2016). Astrocytes in physiological aging and Alzheimer's disease. *Neuroscience*, *323*, 170–182. http://doi.org/10.1016/j.neuroscience.2015.01.007.

Rodriguez-Callejas, J. D., Fuchs, E., & Perez-Cruz, C. (2016). Evidence of tau hyperphosphorylation and dystrophic microglia in the common marmoset. *Frontiers in Aging Neuroscience*, *8*(315), 1–15. http://doi.org/10.3389/fnagi.2016.00315.

Rosas-Arellano, A., Villalobos-González, J. B., Palma-Tirado, L., Beltrán, F. A., Cárabez-Trejo, A., Missirlis, F., & Castro, M. A. (2016). A simple solution for antibody signal enhancement in immunofluorescence and triple immunogold assays. *Histochemistry and Cell Biology*, *146*(4), 421–430. http://doi.org/10.1007/s00418-016-1447-2.

Ross, C. N., & Salmon, A. B. (2018). Aging research using the common marmoset: Focus on aging interventions. *Nutrition and Healthy Aging*, 1–13. http://doi.org/10.3233/NHA-180046.

Sadoun, A., Rosito, M., Fonta, C., & Girard, P. (2018). Key periods of cognitive decline in a non-human primate model of cognitive aging, the common marmoset (Callithrix jacchus). *Neurobiology of Aging*, *74*, 1–14. http://doi.org/10.1016/j.jfoodeng.2018.03.029.

Sadoun, A., Strelnikov, K., Bonté, E., Fonta, C., & Girard, P. (2015). Cognitive impairment in a young marmoset reveals lateral ventriculomegaly and a mild hippocampal atrophy: A case report. *Scientific Reports*, *5*(16046), 1–11. http://doi.org/10.1038/srep16046.

Salminen, A., Kaarniranta, K., & Kauppinen, A. (2012). Inflammaging: Disturbed interplay between autophagy and inflammasomes. *Aging*, *4*(3), 166–175. http://doi.org/10.18632/aging.100444.

Sands, S. A., Leung-Toung, R., Wang, Y., Connelly, J., & LeVine, S. M. (2016). Enhanced histochemical detection of iron in paraffin sections of mouse central nervous system tissue: Application in the APP/PS1 mouse model of Alzheimer's disease. *ASN Neuro*, *8*(5), http://doi.org/10.1177/1759091416670978.

Schäfer, S., Wirths, O., Multhaup, G., & Bayer, T. A. (2007). Gender dependent APP processing in a transgenic mouse model of Alzheimer's disease. *Journal of Neural Transmission*, *114*(3), 387–394. http://doi.org/10.1007/s00702-006-0580-9.

Shan, X., Chang, Y., & Lin, C. L. (2007). Messenger RNA oxidation is an early event preceding cell death and causes reduced protein expression. *The FASEB Journal*, *21*(11), 2753–2764. http://doi.org/10.1096/fj.07-8200com.

Shan, X., & Lin, C. G. (2006). Quantification of oxidized RNAs in Alzheimer's disease. *Neurobiology of Aging*, *27*(5), 657–662. http://doi.org/10.1016/j.neurobiolaging.2005.03.022.

Smith, M. A., Harris, P. L., Sayre, L. M., & Perry, G. (1997). Iron accumulation in Alzheimer disease is a source of redox-generated free radicals. *Proceedings of the National Academy of Sciences of the United States of America*, *94*(18), 9866–9868. http://doi.org/10.1073/pnas.94.18.9866.

Smith, M. A., Rottkamp, C. A., Nunomura, A., Raina, A. K., & Perry, G. (2000). Oxidative stress in Alzheimer's disease. *Biochimica Et Biophysica Acta (BBA) − Molecular Basis of Disease*, *1502*(1), 139–144. http://doi.org/10.1016/S0925-4439(00)00040-5.

Spittau, B. (2017). Aging microglia-phenotypes, functions and implications for age-related neurodegenerative diseases. *Frontiers in Aging Neuroscience*, *9*(194), 1–9. http://doi.org/10.3389/fnagi.2017.00194.

Splettstoesser, W. D., & Schuff-Werner, P. (2002). Oxidative stress in phagocytes − "The enemy within." *Microscopy Research and Technique*, *57*(6), 441–455. http://doi.org/10.1002/jemt.10098.

Streit, W. J., Braak, H., Xue, Q. S., & Bechmann, I. (2009). Dystrophic (senescent) rather than activated microglial cells are associated with tau pathology and likely precede neurodegeneration in Alzheimer's disease. *Acta Neuropathologica*, *118*(4), 475–485. http://doi.org/10.1007/s00401-009-0556-6.

Streit, W. J., Sammons, N. W., Kuhns, A. J., & Sparks, D. L. (2004). Dystrophic microglia in the aging human brain. *Glia*, *45*(2), 208–212. http://doi.org/10.1002/glia.10319.

Streit, W. J., & Xue, Q.-S. (2016). Microglia in dementia with Lewy bodies. *Brain, Behavior, and Immunity*, *55*(2016), 191–201. http://doi.org/10.1016/j.bbi.2015.10.012.

Streit, W. J., Xue, Q.-S., Tischer, J., & Bechmann, I. (2014). Microglial pathology. *Acta Neuropathologica Communications*, *2*, 142. http://doi.org/10.1186/s40478-014-0142-6.

Syslová, K., Böhmová, A., Mikoska, M., Kuzma, M., Pelclová, D., & Kacer, P. (2014). Multimarker screening of oxidative stress in aging. *Oxidative Medicine and Cellular Longevity*, *2014*(562860), 1–14. http://doi.org/10.1155/2014/562860.

T'Hart, B. A., Abbott, D. H., Nakamura, K., & Fuchs, E. (2012). The marmoset monkey: A multi-purpose preclinical and translational model of human biology and disease. *Drug Discovery Today*, *17*(21–22), 1160–1165. http://doi.org/10.1016/j.drudis.2012.06.009.

Tang, Y., & Le, W. (2016). Differential roles of M1 and M2 microglia in neurodegenerative diseases. *Molecular Neurobiology*, *53*(2), 1181–1194. http://doi.org/10.1007/s12035-014-9070-5.

Tardif, S. D., Mansfield, K. G., Ratnam, R., Ross, C. N., & Ziegler, T. E. (2011). The marmoset as a model of aging and age-related diseases. *ILAR Journal*, *52*(1), 54–65. http://doi.org/10.1016/j.biotechadv.2011.08.021.

Tremblay, M.-, Zettel, M. L., Ison, J. R., Allen, P. D., & Majewska, A. K. (2012). Effects of aging and sensory loss on glial cells in mouse visual and auditory cortices. *Glia*, *60*(4), 541–558. http://doi.org/10.1002/glia.22287.

Vernon, P. J., & Tang, D. (2013). Eat-me: Autophagy, phagocytosis, and reactive oxygen species signaling. *Antioxidants & Redox Signaling*, *18*(6), 677–691. http://doi.org/10.1089/ars.2012.4810.

von Bernhardi, R., Eugenín-von Bernhardi, L., & Eugenín, J. (2015). Microglial cell dysregulation in brain aging and neurodegeneration. *Frontiers in Aging Neuroscience*, *7*(124), 1–21. http://doi.org/10.3389/fnagi.2015.00124.

Walker, T., Michaelides, C., Ekonomou, A., Geraki, K., Parkes, H. G., Suessmilch, M., ... So, P. W. (2016). Dissociation between iron accumulation and ferritin upregulation in the aged substantia nigra: Attenuation by dietary restriction. *Aging*, *8*(10), 2488–2508. http://doi.org/10.18632/aging.101069.

Wang, J., Tanila, H., Puoliväli, J., Kadish, I., & Van Groen, T. (2003). Gender differences in the amount and deposition of amyloidβ in APPswe and PS1 double transgenic mice. *Neurobiology of Disease*, *14*(3), 318–327. http://doi.org/10.1016/j.nbd.2003.08.009.

Wang, L., Yang, H., Zhao, S., Sato, H., Konishi, Y., Beach, T. G., ... Tooyama, I. (2011). Expression and localization of mitochondrial ferritin mRNA in Alzheimer's disease cerebral cortex. *PLoS ONE*, *6*(7), 1–8. http://doi.org/10.1371/journal.pone.0022325.

Ward, R. J., Zucca, F. A., Duyn, J. H., Crichton, R. R., & Zecca, L. (2014). The role of iron in brain ageing and neurodegenerative disorders. *The Lancet Neurology*, *13*(10), 1045–1060. http://doi.org/10.1016/S1474-4422(14)70117-6.

Workman, K. P., Healey, B., Carlotto, A., & Lacreuse, A. (2018). One-year change in cognitive flexibility and fine motor function in middle-aged male and female marmosets (Callithrix jacchus). *American Journal of Primatology*, e22924. http://doi.org/10.1002/ajp.22924.

Xue, Q. S., & Streit, W. J. (2011). Microglial pathology in Down syndrome. *Acta Neuropathologica*, *122*(4), 455–466. http://doi.org/10.1007/s00401-011-0864-5.

Zecca, L., Youdim, M. B. H., Riederer, P., Connor, J. R., & Crichton, R. R. (2004). Iron, brain ageing and neurodegenerative disorders. *Nature Reviews Neuroscience*, *5*(11), 863–873. http://doi.org/10.1038/nrn1537.

Zhang, J., Perry, G., Smith, M. A., Robertson, D., Olson, S. J., Graham, D. G., & Montine, T. J. (1999). Parkinson's disease is associated with oxidative

damage to cytoplasmic DNA and RNA in substantia nigra neurons. *The American Journal of Pathology*, *154*(5), 1423–1429. http://doi.org/10.1016/S0002-9440(10)65396-5.

SUPPORTING INFORMATION

Additional supporting information may be found online in the Supporting Information section at the end of the article.